

2007-11

# Neural Dynamics of Saccadic and Smooth Pursuit Eye Movement Coordination during Visual Tracking of Unpredictably Moving Targets

---

<https://hdl.handle.net/2144/1956>

*"Downloaded from OpenBU. Boston University's institutional repository."*

# Neural dynamics of saccadic and smooth pursuit eye movement coordination during visual tracking of unpredictably moving targets

Stephen Grossberg, Krishna Srihasam, and Daniel Bullock<sup>1</sup>

Department of Cognitive and Neural Systems,  
Center for Adaptive Systems  
and  
Center of Excellence for Learning in Education, Science and Technology  
Boston University  
677 Beacon Street, Boston, MA 02215

Submitted November, 2007  
**CAS/CNS Technical Report 2007-018**

*All correspondence should be addressed to*  
Professor Stephen Grossberg  
Department of Cognitive and Neural Systems  
Boston University  
677 Beacon Street  
Boston, MA 02215  
Phone: 617-353-7858  
Fax: 617-353-7755  
Email: [steve@bu.edu](mailto:steve@bu.edu)

---

<sup>1</sup> Authorship is in rotated alphabetical order. DB, SG and KS were supported in part by NSF grant SBE-0354378. SG was also supported in part by the office of Naval Research (ONR N00014-01-1-0624).

Copyright © 2007

Permission to copy without fee all or part of this material is granted provided that: 1. The copies are not made or distributed for direct commercial advantage; 2. the report title, author, document number, and release date appear, and notice is given that copying is by permission of the BOSTON UNIVERSITY CENTER FOR ADAPTIVE SYSTEMS AND DEPARTMENT OF COGNITIVE AND NEURAL SYSTEMS. To copy otherwise, or to republish, requires a fee and / or special permission.

**Abstract**

How does the brain use eye movements to track objects that move in unpredictable directions and speeds? Saccadic eye movements rapidly foveate peripheral visual or auditory targets and smooth pursuit eye movements keep the fovea pointed toward an attended moving target. Analyses of tracking data in monkeys and humans reveal systematic deviations from predictions of the simplest model of saccade-pursuit interactions, which would use no interactions other than common target selection and recruitment of shared motoneurons. Instead, saccadic and smooth pursuit movements cooperate to cancel errors of gaze position and velocity, and thus to maximize target visibility through time. How are these two systems coordinated to promote visual localization and identification of moving targets? How are saccades calibrated to correctly foveate a target despite its continued motion during the saccade? A neural model proposes answers to such questions. The modeled interactions encompass motion processing areas MT, MST, FPA, DLPN and NRTP; saccade planning and execution areas FEF and SC; the saccadic generator in the brain stem; and the cerebellum. Simulations illustrate the model's ability to functionally explain and quantitatively simulate anatomical, neurophysiological and behavioral data about SAC-SPEM tracking.

**Key Words:** saccade, smooth pursuit, oculomotor, MT, MST, FEF, superior colliculus, DLPN, NRTP, cerebellum, step-ramp paradigm

## Introduction

To visually examine an object in the environment, we move our fovea to it using two types of eye movements: Saccadic eye movements (SAC) shift the fovea rapidly to a peripheral visual or auditory target, and smooth pursuit eye movements (SPEM) keep the image of an attended moving target near the fovea. The SAC system uses positional error – the retinal error between the target and the fovea – as a signal to set the direction and amplitude of a saccade. When the target is moving, the positional error continuously varies if the eye and target velocity are different, thereby leading to a target-related retinal slip. The SPEM system uses the velocity of retinal slip as a sensory signal for tracking the target in space. However, retinal slip this signal alone is insufficient for maintaining SPEM because target slip becomes zero whenever eye velocity matches target velocity.

This paper introduces a model of how these two eye movement systems are intelligently coordinated to maintain foveation on an object of interest. Due to delays in the visual system and SPEM velocity saturation (inability of the oculomotor system to track smoothly at high speeds), tracking a moving target often requires a “catch-up” saccade to refoveate the target. How are these two systems coordinated to promote visual localization and scrutiny of moving targets? Unnecessary catch-up saccades should be avoided, because vision is degraded during a saccade. How does the brain make the decision to initiate a saccade while smoothly pursuing a target? How does the SPEM system interact with the saccadic system to improve that decision? Are saccades to moving targets calibrated differently than saccades to stationary targets? What happens to the SPEM command when the subject generates a SAC command?

The smooth pursuit and saccadic systems have often been treated as separate and parallel systems interacting at only two stages: target selection and the motoneurons that control the eye muscles. Recent data quantify how SAC and SPEM interact in the normal course of eye movements. Data from monkeys performing the Rashbass paradigm (Rashbass, 1961) show that information about target motion, not just about target position, influences SAC decisions. In this paradigm, ramp motion of a target immediately follows an abrupt step of target position in the opposite direction. By manipulating the size of the step and/or the speed of the ramp motion, the paradigm induces a monkey to initiate a catch-up saccade or to begin pursuit without an initial saccade. Notably, catch-up saccades depend on both the target’s step size and ramp speed thereafter (de Brouwer, Missal, Barnes, & Lefevre, 2002; de Brouwer, Missal, & Lefevre, 2001; de Brouwer, Yuksel, Blohm, Missal, & Lefevre, 2002).

Existing models of saccadic eye movement (Brown, Bullock, & Grossberg, 2004; Dominey & Arbib, 1992; Droulez & Berthoz, 1991; Gancarz & Grossberg, 1999; Grossberg & Kuperstein, 1986; Grossberg, Roberts, Aguilar, & Bullock, 1997; Optican & Quaia, 2002; Waitzman, Ma, Optican, & Wurtz, 1991) exclusively treat the control of saccades. The Grossberg et al. (1997) model predicts how a multi-modal map is learned in superior colliculus (SC), such that visual, auditory and planned representations of target positions become aligned in retinal coordinates. It and Brown et al. (2004) also treat how voluntary gating by substantia nigra determines whether excitation of an SC map locus leads to genesis of a corresponding saccade. Gancarz and Grossberg (1999) proposed how several brain regions work together to control and adapt saccades in response to different conditions, notably how the cerebellum (CBM) adapts saccadic gain in a context-sensitive way. Optican and Quaia (2002) proposed that the SC encodes the desired sensory consequence of the saccade in retinotopic coordinates. Their model cerebellum (CBM) learns to use contextual information (like initial eye positions, target velocity)

and movement errors to initialize a “pilot” signal that will guide the saccade to its goal. In particular, the CBM generates a burst of activity in the contralateral oculomotor region of the fastigial nucleus (FOR) and this activity spreads, with a speed proportional to the velocity of the eyes, from the contralateral to the ipsilateral FOR. To generate the burst, NRTP (which acts as way station between SC and FOR) was connected to the FOR in a topographically organized manner. The vermis then monitors feedback information from brain stem about saccade velocity to steer and stop the saccade by inhibiting the FOR. This replaces the classical notion of a displacement integrator (Jurgens, Becker, & Kornhuber, 1981), which uses the desired change in eye position instead of the desired eye position as an input to the saccade generator. A major difference between the Optican and Quaia (2002) and Gancarz and Grossberg (1999) models lies in how the CBM corrects for saccadic errors. The Optican and Quaia model converts a feedback signal about saccade velocity into a retinotopically organized map in vermis. Any deviation from the original path (such as a directional deviation, overshoot, or undershoot) is corrected online. In the Gancarz and Grossberg model, gain learning helps the CBM compensate for saccadic errors as buildup cells in the SC steer the eye towards the target.

The smooth pursuit model of Pack et al. (2001) investigated interactions between cells in the ventral and dorsal subdivisions of cortical area MST, which processes target velocity and background motion (Newsome, Wurtz, & Komatsu, 1988). The model addresses a number of behavioral phenomena related to SPEM and target velocity. The model proposes how visual background counter-motion generated during SPEM is computed in  $MST_D$  and combines with retinal slip and corollary discharge signals in  $MST_V$  to generate a predicted target speed command. The model simulates behavioral data about pursuit maintenance and perceptual data from human studies, including the Aubert--Fleischl phenomenon and the Filehne Illusion.

The Robinson et al. (1986) model also used an efference copy of eye velocity added to the target's retinal slip to construct an internal representation of predicted target velocity that persists even if retinal slip is zero, but this model did not include background counter-motion. To complete such models, it is necessary to adaptively calibrate the gains of SPEM commands. Several kinds of cerebellum-mediated adaptation within a Robinson-type pursuit model were simulated in Arakawa (2003), notably adaptation that adjusted gains while also compensating for time delays. However, none of these models addressed SAC-SPEM interactions.

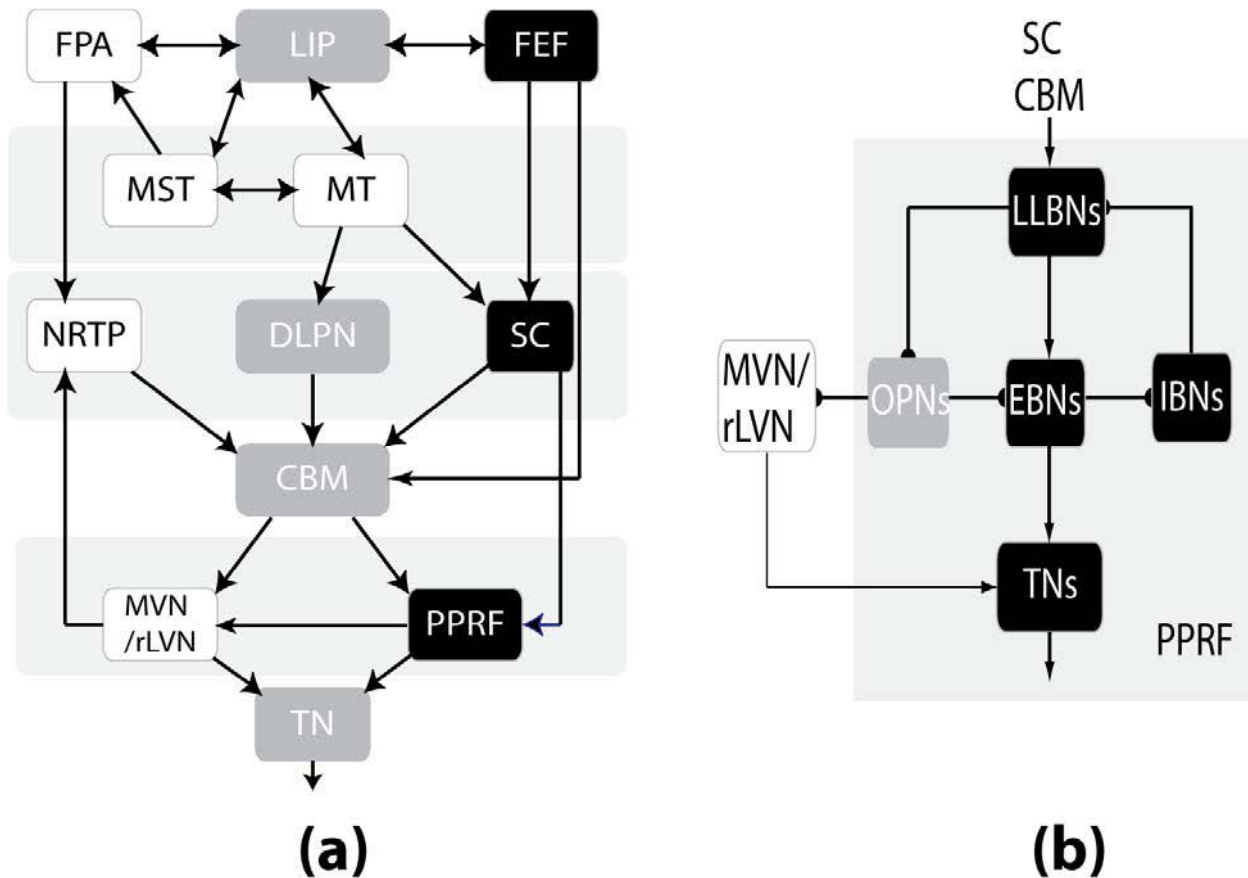


**Figure 1. Modeled interactions among brain regions implicated in oculomotor control.** (a) Black boxes denote areas belonging to the saccadic eye movement system (SAC), white boxes the smooth pursuit eye-movement system (SPEM), and gray boxes, both systems. LIP – Lateral Intra-Parietal area; FPA – Frontal Pursuit Area; MST – Middle Superior Temporal area; MT – Middle Temporal area; FEF – Frontal Eye Fields; NRTP – Nucleus Reticularis Tegmenti Pontis; DLPN - Dorso-Lateral Pontine Nuclei; SC - Superior Colliculus; CBM – cerebellum; MVN/rLVN – Medial and Rostro-Lateral Vestibular Nuclei; PPRF – a Peri-Pontine Reticular Formation; TN – Tonic Neurons. (b) Constituents of the saccade generator in the PPRF, and projection of omnipauseur neurons to the pursuit neurons of the MVN/rLVN. Arrows indicate excitatory connections, and semi-circles indicate inhibitory connections. OPN - Omni-Pauseur Neurons; LLBN – Long-Lead Burst Neuron; EBN- Excitatory Burst Neuron; IBN – Inhibitory Burst Neuron; TN - Tonic Neurons.

### Model Overview

The model (Figure 1) consists of two parallel yet interacting processing streams to control SAC and SPEM movements. It unified and further developed the SAC model Grossberg et al., (1997) and Gancarz and Grossberg (1999), and the SPEM model of Pack et al., (2001). Table 1 summarizes the neuroanatomical connections and their functional interpretation, discussed below, that are unified within this model. A complete mathematical specification of the model and simulation details are provided in the Appendix. Model results were briefly reported in Srihasam, Bullock, & Grossberg (2005, 2006a, 2006b, 2007).

*The SPEM stream.* The model's smooth pursuit stream contains visual area MT-like cell types (Figure 1), which are selective to the direction and speed of visual stimuli that fall within their retinotopic receptive fields (Albright, 1984; Maunsell & Van Essen, 1983). The 800 model MT cells (described in equations (9) and (12)) provide inputs to the model's MST cells, which pool MT inputs to become direction-selective and speed-sensitive, but not speed-selective.

Because these MST cells also receive corollary discharge inputs corresponding to current eye velocity from MVN cells (Figure 1a), they can compute an internal estimate of target velocity (as described in equations (13) and (15)) that remains accurate even as eye velocity grows to match target velocity, and thus gradually cancels the target-related retinal image motion that drives MT cells.

The robust estimate of target velocity computed by model MST cells provides a key basis for the model's frontal cortical representation of desired pursuit velocity. In particular, the frontal pursuit area (FPA), at the rostral bank of the arcuate sulcus, receives strong inputs from MST (Huerta, Krubitzer, & Kaas, 1987; Tian & Lynch, 1996a, 1996b). Model and real FPA cells have high direction-selectivity and speed-sensitivity, but almost no speed-selectivity (Gottlieb, Bruce, & MacAvoy, 1993; Tanaka & Lisberger, 2002b).

The model FPA cells (described in equations (16) – (19)) project (Brodal, 1980a; Giolli et al., 2001) to the model NRTP (nucleus reticularis tegmenti pontis) which includes two types of cells: acceleration and velocity cells (Ono, Das, Economides, & Mustari, 2005; Ono, Das, & Mustari, 2004; Suzuki, Yamada, Hoedema, & Yee, 1999; T. Yamada, Suzuki, & Yee, 1996). Model NRTP velocity cells (described in equation (23)) integrate the output of NRTP acceleration cells (described in equation (22)). The latter compute the difference between an excitatory target-velocity command from FPA and an inhibitory eye-velocity signal from MVNs. This inhibitory process is predicted but has no direct data support at present. The computed difference estimates the eye acceleration needed to match target velocity. These two classes of cells allow the NRTP to play a key role in SPEM initiation.

Parallel to the FPA-NRTP pathway, a second pathway exists for the transmission of SPEM-related information from the cortex to the cerebellum via the pons: Model MT cells project to DLPN (dorsal lateral pontine nucleus) cells of the brain stem. The DLPN cells have been implicated in maintenance of SPEM (Mustari, Fuchs, & Wallman, 1988; Suzuki & Keller, 1984). In the model, the DLPN cells have similar speed and directional selectivities as MT cells, but they lack their retinotopic specificity (see equation (21)).

*The saccadic stream.* In the model saccadic system, retinotopically organized visual signals are processed to produce saccadic target choices in the model SC (superior colliculus, see equations (30) – (45)), LIP (lateral intra-parietal area, equation (59)), and FEF (frontal eye fields, equations (48) – (57)). FEF outputs serve as inputs to corresponding retinotopic loci in two layers of the motor error map of the model's SC (superior colliculus). There is also communication between the two SC layers. In particular, activated loci in the *burst cell* layer (described in equation (30)) excite corresponding cells in the *buildup cell* layer (described in equation (35)) of the SC (cf., Grossberg et al., 1997).

Outputs from the SC reach the cerebellum and the saccade generator circuit (Figure 1b) in the para-median pontine reticular formation (PPRF), which contains populations of SAC- and SPEM-related cells, some of which provide direct input to the oculomotor neurons that innervate eye muscles. Model saccadic control signals from cerebellar and SC stages converge at model long-lead burst neurons (LLBN). The LLBN activity (described in equation (73)) encodes the gaze-position error and these cells excite corresponding excitatory burst neurons (EBNs). The model EBNs (described in equation (74)) project to the tonic neurons (TNs), which integrate inputs from EBNs and excite the model oculomotor neurons. The EBNs also excite inhibitory burst neurons (IBNs), which in turn inhibit the LLBNs, thereby completing an internal negative feedback loop that controls ballistic saccades (see equation (75)). Except during saccades, the

EBNs receive strong inhibition from model omni-pause neurons (OPNs), so-called because they pause deeply to disinhibit saccades of all directions (see citations in Table 1).

*Shared omni-pausers.* In the brain, OPNs are located in the nucleus raphe interpositus (Buttner-Ennever & Horn, 1997; Langer & Kaneko, 1990). The pursuit neurons (PNs) found in the vestibular nuclei (MVN/rLVN) are modeled as receiving input from the cerebellum and projecting directly to the TNs, which are thus shared by SAC and SPEM systems. The PNs are weakly inhibited by, and themselves inhibit, the OPNs, also shared by both systems. About 50% of the OPNs show 34% reduced activity during smooth pursuit (Missal & Keller, 2002), whereas most OPNs pause more deeply during saccades (Everling et al., 1998; Munoz et al., 2000). Thus the spontaneously active and inhibitory OPNs normally oppose both saccades and SPEM. Shallow pausing by OPNs can release SPEM but not saccades, whose releases require deeper pauses.

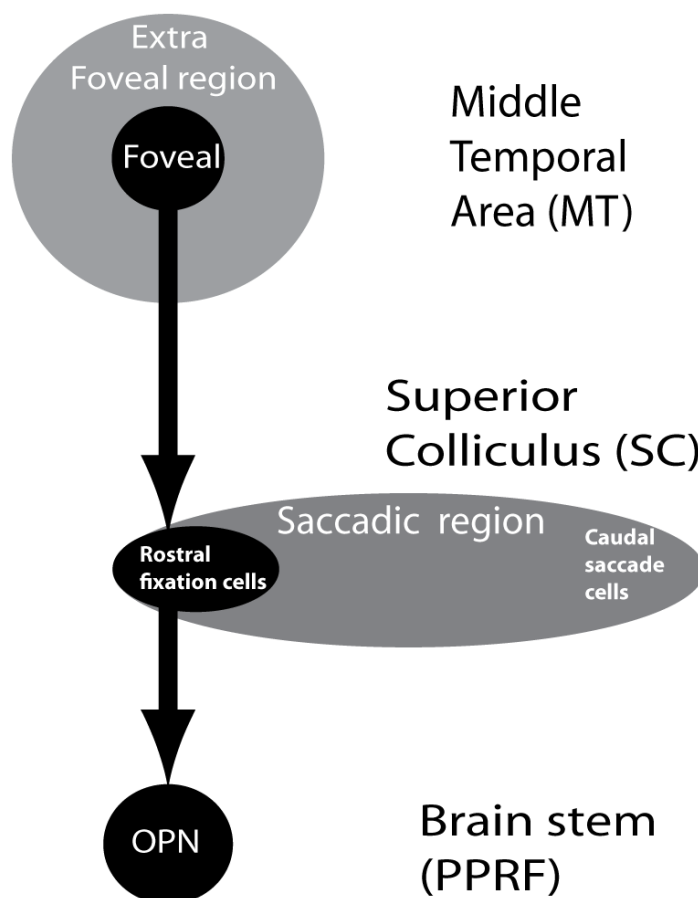


**Figure 2. Cortico-colliculo-reticular control of saccade initiation.** The figure illustrates a pathway from foveal and para-foveal cells in cortical area MT to the rostral pole of the SC and then to the OPNs in the PPRF. Effective tracking causes MT foveal cells to become active. This, in turn, activates fixation cells present in the rostral SC. Such SC cells excite OPNs, which can inhibit saccade initiation or suspend on-going saccades.

*SPEM system inhibition of SAC initiation via an MT–SC–OPN pathway.* Behavioral data (simulated below) suggest the existence of an intelligent mechanism to control saccade initiations during SPEM, notably to inhibit saccades when targets are already foveal or parafoveal. Pursuit-related neural activity is reliably observed in the SC: Rostral parts of SC

(rSC) contain cells that respond to both SPEM and saccadic eye movements (Krauzlis, Basso, & Wurtz, 2000). As schematized in Figure 2, area MT sends strong excitatory projections to rSC (Collins, Lyon, & Kaas, 2005; Davidson & Bender, 1991; Maioli, Domeniconi, Squatrito, & Riva Sanseverino, 1992; Spatz & Tigges, 1973), which in turn provides the main excitatory input to the OPNs (Everling, Pare, Dorris, & Munoz, 1998; Gandhi & Keller, 1997; Pare & Guitton, 1994). In the model (Figures 1 and 2), foveal and para-foveal cells in area MT, which are active when pursued targets are on or near the fovea, inhibit saccades via an excitatory pathway from MT to rSC to the OPNs.

*Cerebellar learning calibrates SPEM and SAC commands.* Learning is needed to keep SAC and SPEM metrics accurate as eye muscles and other system parameters change. Inactivation or lesion of the cerebellum causes deficits in the ability to adapt both saccadic and smooth pursuit eye movements (Takagi, Zee, & Tamargo, 1998). Each output cell in the retinotopic model FEF (equation (63)), SC (equation (62)), each speed-sensitive cell in the model DLPN (equation (21)), and each direction-sensitive cell in the model NRTP (equation (23)) sends signals to the cerebellum (Thier & Ilg, 2005). These signals are modified by adaptive weights learned within the cerebellum. The weighted saccade-related cerebellar outputs (described in equation (70)) reach the model para-median pontine reticular formation (PPRF) region of the brain stem (Figure 1a), the location of the saccade generator (Figure 1b). Similarly, the weighed pursuit-related cerebellar outputs reach the pursuit neurons (PNs) in the medial and rostra-lateral vestibular nuclei (MVN/ rLVN) of the brain stem (Figure 1a).

### **Results: Model of Simulations of SAC-SPEM Data**

*Simulation 1: Threshold for catch-up saccades.* During sustained pursuit of a target, the target may undergo an unexpected step change in position and velocity (de Brouwer, Yuksel et al., 2002). In general, catch-up saccades follow these unexpected steps in position and velocity of the target. Catch-up saccades occur in the same direction as the smooth eye movement (forward saccades) as well as in the opposite direction (reverse saccades). Parametric studies (de Brouwer, Yuksel et al., 2002; Tanaka, Yoshida, & Fukushima, 1998) show that the size and direction of the step in position controls the generation of the catch-up saccades. If the size of the position step is small and is in a direction opposite to target motion, catch-up saccades are generally omitted (de Brouwer, Missal et al., 2002; Missal & Keller, 2002). That is, saccades are not reflexively generated to modest position errors during SPEM.

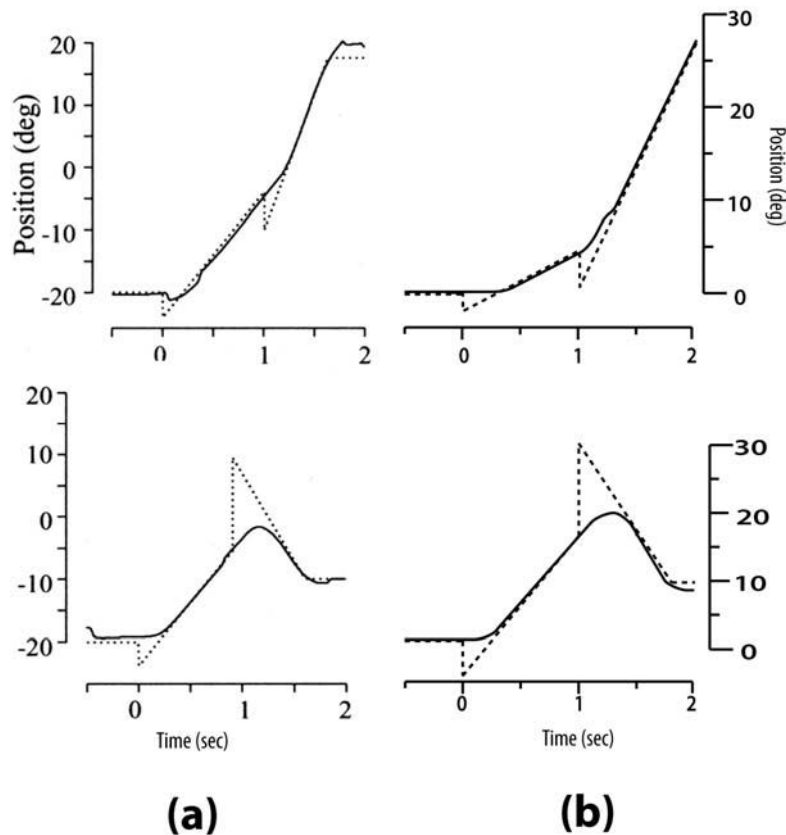


**Figure 3. Step-ramp paradigms illustrate dual control of saccade decisions: Data and simulations.** The left column (a) shows data from humans exposed to step-ramp paradigms (reprinted, with permission, from de Brouwer et al., 2002). The right column (b) shows model simulation results that replicate performance in these experimental paradigms. For both simulations (top and bottom panels), the target initially jumped  $3^\circ$  left and started moving rightwards with a speed of  $20^\circ/\text{s}$ . For the top panel, At  $t = 2000$ , the target again jumped by  $5^\circ$  left and started moving leftwards with a speed of  $30^\circ/\text{s}$ . For the bottom panel, the target again jumped by  $5^\circ$  right and started moving leftwards with a speed of  $30^\circ/\text{s}$ . Each panel shows horizontal target position (dotted trace) and gaze-position (continuous trace) versus time. Once foveation of a target is achieved, a step change in either position or speed, or both, unexpectedly occurs. The top row shows, near  $t=1$ , a backward step in position, i.e., in a direction opposite to the prior target motion and SPEM. That target step is followed by continued target motion in the original direction, but at a reduced speed. A large, backward (downward in plot), catch-up saccade occurs after the step. The middle row shows a backward step that is followed by continued target motion in the original direction, but at increased speed. This combination does not induce a catch-up saccade. The bottom row shows a step along the direction of prior target motion, followed by a reversal of target motion direction. This combination also induces no catch-up saccade. Thus, even in the presence of a significant gaze-position error, a saccade is usually omitted when the target's motion is reducing the error and is therefore likely to render the saccade unnecessary.

The modeled projection from MT to SC to the OPNs helps replicate several behavioral characteristics observed in the step-ramp paradigm. It is well established (de Brouwer, Missal et al., 2002; Rashbass, 1961; Van Gelder, Lebedev, & Tsui, 1995, 1997) that, by controlling the size of the jump and the velocity of target motion after the jump, the occurrence or non-occurrence of catch-up saccades can be manipulated. Figure 3a shows representative data and Figure 3b simulations of these data. In the top row, the target (dotted lines) first jumps and then starts moving in a direction opposite to that of the prior jump. There is a second step-ramp episode later on, with a larger jump and faster post-jump ramp. Both the first and second step-ramp combination do not elicit a saccade. Two mechanisms help achieve this: First, during near

accurate pursuit (target is within  $\pm 1.5^\circ$  of the fovea), the OPNs inhibit any saccades that might be initiated due to presence of the small positional error or transient flashes (Figure 2). Second, as the target starts moving towards the fovea during the ramp phase after the step, the positional error, even if initially large, starts to fall. The rate of reduction in positional error depends on the velocity of the target. A target moving towards the fovea will not initiate a saccade if the target enters the para-foveal or foveal region within the latency needed to initiate a saccade. The steps in rows one and two in Figure 3 thus elicit no saccades because the high-velocity post-step ramps bring the target near enough to the fovea to engage rSC excitation of OPNs before expiration of the latency needed to initiate a saccade. The same factors help explain observations (Rashbass, 1961; Tanaka et al., 1998) that saccades to targets moving towards the fovea are more likely to be cancelled than those made to targets moving away from the fovea.

Because of the weaker effect of OPN inhibition on SPEM than on saccades, it is possible in the model for rSC activation during pursuit to suppress saccades without significantly inhibiting SPEM. This is consistent with observations that, during pursuit initiation, artificial stimulation of the rSC has only modest effects on contra-versive SPEM although it suppresses ipsi-versive SPEM. One possible explanation for the ipsi-versive inhibition comes from the fact that anti-dromic input from SC might reach MT (via pulvinar) and cancel the visual input present at that location. The effect of stimulation varied, such that most rostral sites produced the most inhibition of ipsi-versive pursuit (Basso, Krauzlis, & Wurtz, 2000). Such artificial stimulation was more effective on higher pursuit speeds.

*Simulation 2: Post-saccadic enhancement of pursuit motion.* Tracking a moving stimulus from rest usually initiates a period of smooth pursuit followed by a catch-up saccade, which brings the eye close to the position of the target. Immediately after the saccade, the eye velocity closely matches that of the target even though the pre-saccadic eye velocities were very low (Lisberger, 1998). This phenomenon has been called “post-saccadic enhancement” of SPEM. Lisberger (1998) proposed that saccades activate a switch that controls the strength of activation (or gain) of the pursuit pathway. Therefore, if pursuit is initiated without a saccade – i.e. with this switch “closed” – the pursuit system takes more time to reach target velocity, consistent with observations (Lisberger, 1998). For reasons already cited above, the OPNs are well suited to mediate the post-saccadic enhancement because model OPNs pause moderately during SPEM but deeply during saccades. We posit that, for such a gain switch to improve overall performance, it should operate within an internal negative feedback loop (Figure 4) which prevents the eye velocity command that results from enhanced gain in the pursuit pathway from increasing much beyond the current estimate of target velocity.

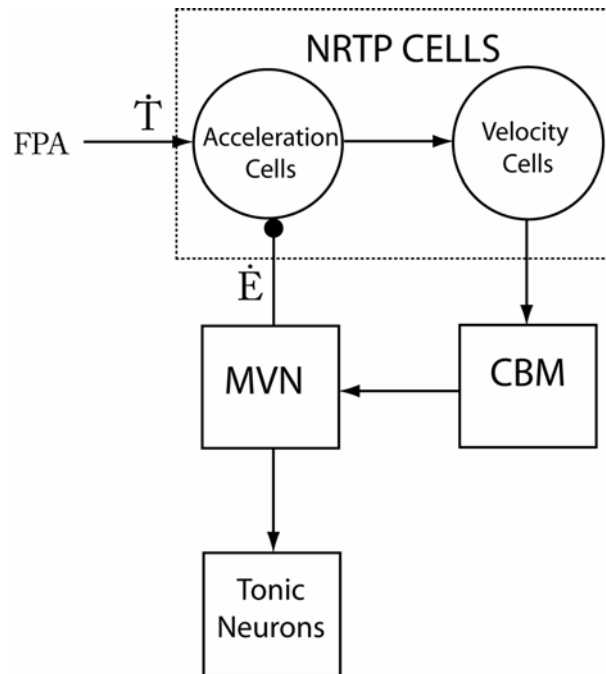


**Figure 4. Sustained pursuit and integration of acceleration signals in NRTP.** In the model, sustained pursuit is possible even if successful SPEM drives the retinal slip rate to zero, because pursuit is guided by a cortical estimate of target velocity, not by retinal slip as such. To update the SPEM velocity command, the model utilizes an internal negative feedback loop to compute the difference between the cortical estimate of target velocity and the currently commanded eye velocity, which strongly depends on learned cerebellar inputs to the vestibular nuclei. The computed difference between two velocity estimates yields a desired acceleration signal, which must be integrated to form a sustained command for desired SPEM velocity. The model NRTP performs differencing and integration to create both acceleration and velocity cells, and with the NRTP's receipt of high-level velocity-related signals from the FPA (frontal pursuit area) and low-level velocity-related signals from the MVN (medial vestibular nucleus). The model NRTP acceleration cells thus act as a comparator between the estimated target velocity and estimated eye velocity. The output from these cells is integrated by the model NRTP's velocity neurons

What anatomical substrates realize these mechanisms? In particular, NRTP contains gaze acceleration and gaze velocity cells (Ono et al., 2005; Ono et al., 2004; Suzuki et al., 1999; Suzuki, Yamada, & Yee, 2003; T. Yamada et al., 1996) that act as velocity-comparison and velocity integrator cells (Figure 4). These cell types operate as follows in the model: Model FPA cells output to the NRTP of the brain stem (Brodal, 1980a, 1980b; Giolli et al., 2001). The vestibular nuclei (MVN/rLVN), whose efferents control pursuit eye movements, also send collateral signals to NRTP (Torigoe, Blanks, & Precht, 1986). These efference copies are extra-retinal signals indicative of the current eye velocity. NRTP acceleration cells subtract this eye velocity estimate from the current target velocity estimate generated by the FPA output cells. NRTP velocity cells then integrate the activity of NRTP acceleration cells. Any mismatch between the current eye velocity and estimated target velocity generates a compensatory signal that pushes the current eye velocity towards the estimated target velocity. Thus post-saccadic enhancement operates within a circuit that is capable of accurately matching eye velocity to predicted target velocity.

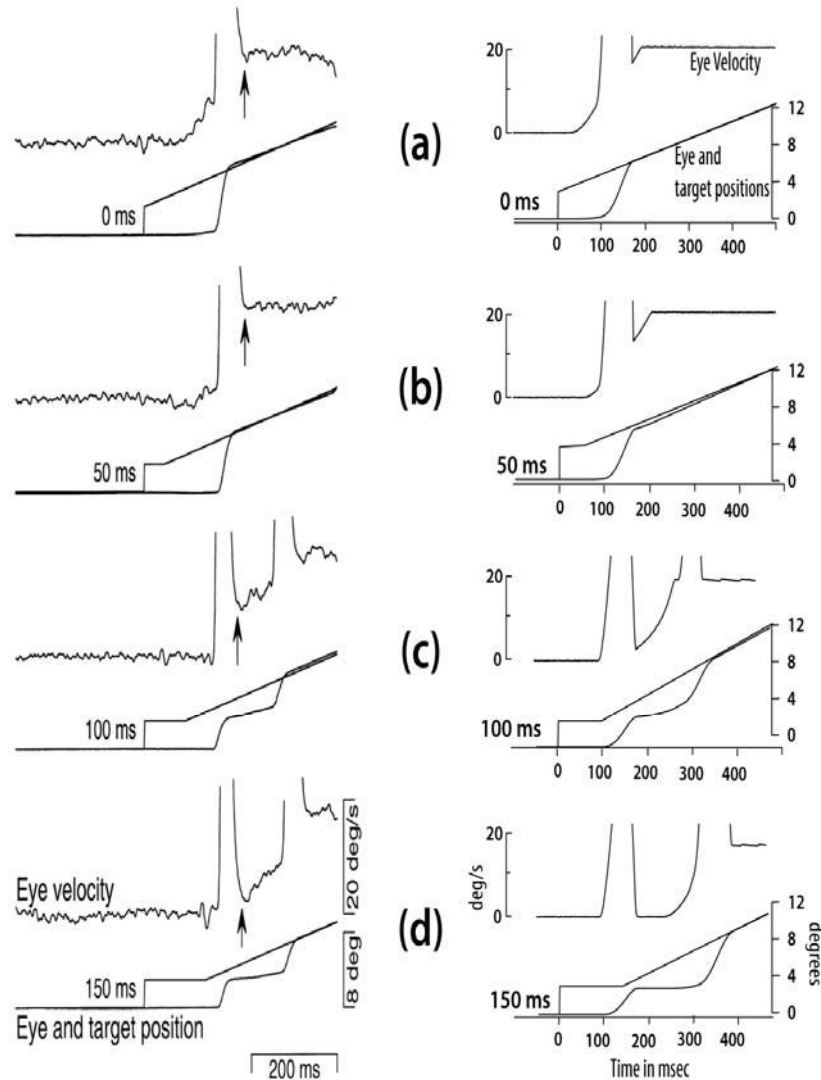


**Figure 5. Saccadic enhancement of the rate of change of pursuit velocity.** The time it takes to make a transition from one SPEM velocity to another depends on saccadic activity. The rate of change of SPEM velocity during a saccade is higher than during a non-saccadic period. It has been postulated that a switch that is partly controlled by the saccadic pathway modulates the SPEM command. In the model, this interaction arises because OPNs used by the saccadic system also inhibit brainstem neurons that carry the SPEM velocity command (see Figure 1 (b)). Each of panels (a) - (d) in the left column show an eye velocity trace (truncated at the high velocities achieved during saccades) above target position and eye position traces for a monkey performing a variant of the step-ramp paradigm (reprinted, with permission, from Lisberger, 1998). Although the step in position was always  $4^\circ$  and the change in ramp slope (target velocity) was always  $20^\circ/\text{s}$ , in panel (a) the target step onset and the ramp motion onset coincided, in panel (b) the ramp motion was delayed for 50 ms, in panel (c), for 100 ms and in panel (d), for 150 ms. In panels (c) and (d), the SPEM velocity after the first saccade is notably less than the target velocity. The right column shows that model simulation results closely match the data

Figure 5 compares the results of model simulations (right column) with the data (left column, from (Lisberger, 1998)). Panels 5a – 5d show traces of eye velocity, and target and eye positions, for a single target step combined with different motion onset times. In panel 5a, there is no delay between the initial target step and subsequent smooth motion. As the delay between the initial step and the onset of subsequent smooth target motion increases to 50, 100, and 150 ms in 5b –

5d, the pursuit system has decreasing time to estimate the target velocity before saccade initiation. In the model, insufficient time always leads to a velocity underestimate, and this causes reduced post-saccadic eye velocity that is visible in both simulations and data. Longer latencies between target step and motion onset cause hypometric saccades because, as explained below, saccades are pre-adapted to compensate for estimated target motion. This is corrected by a subsequent saccade as seen in 5c and 5d. However, the interval between successive saccades is long enough (Kalesnykas and Hallett, 1994, 1996) that the motion system can accurately estimate target velocity during this interval. At the end of the second, correcting, saccade (cf., Figure 5c and 5d), the pursuit eye velocity can exceed target velocity. But, the proposed negative feedback from rLVN/MVN to NRTP acceleration neurons (Figure 4) limits any such velocity overshoots. Once the SPEM eye velocity exceeds the estimated target velocity, input to the NRTP velocity integrators is cut off and the opposite direction is activated. Such an internal negative feedback also helps explain small steady-state oscillations around the target velocity (cf., Arakawa, 2003; Robinson, Gordon, & Gordon, 1986).

*Simulation 3: MT modulates pursuit gain after a saccade.* In adults, the *pursuit gain*, which is the ratio of eye velocity to target velocity, is usually around 1.0. However, modest deviations above or below unity are often observed in SPEM after saccades, and such departures from unity gain typically compensate for modest foveation errors remaining after the prior saccade. If the saccade overshoots, but by too little to evoke a corrective saccade, a SPEM gain less than one allows the target to catch up to the moving line of gaze. If the saccade undershoots, a SPEM gain above unity allows the line of gaze to catch the target, without a catch-up saccade. Such behavior avoids the loss of visibility that would be entailed if, instead, small gaze position errors were always corrected by saccades. In the model, such “saccadic chatter” is avoided via two complementary mechanisms. First, as noted above, the foveation error must exceed a positive threshold to elicit a saccade. Second, overshoots and undershoots affect the size of the population recruited in area MT, and this population response scales the pursuit gain in a way that compensates for the overshoots and undershoots (Figure 6g). An overshoot, an accurate saccade, and an undershoot, respectively, cause recruitment of (relatively) low, medium, and high numbers of MT cells in the controlling hemisphere. These recruitment levels lead to corresponding pursuit gains, of  $1 - \epsilon$ ,  $\sim 1$ , and  $1 + \epsilon$ , where  $\epsilon$  is a small fraction of 1. A simulation illustrating the latter model property is described in Figure 6.

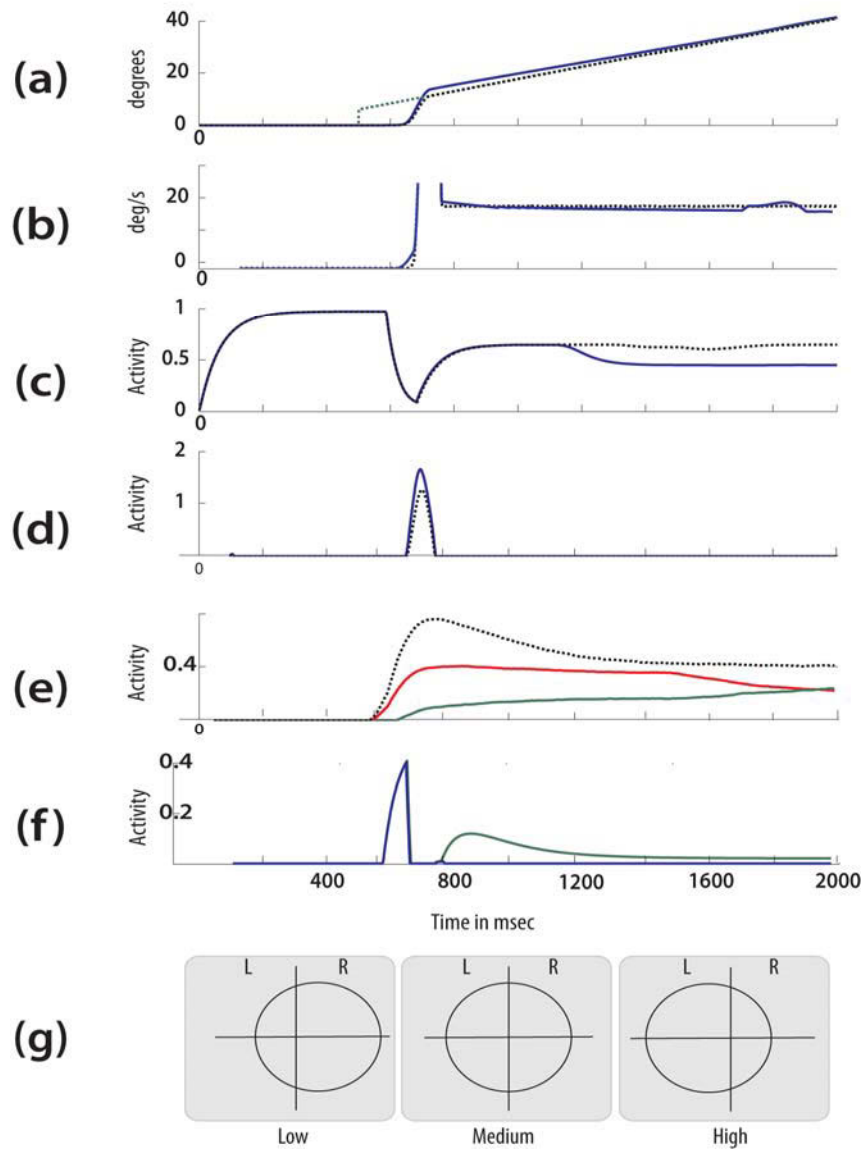


**Figure 6. Pursuit gain drops transiently after a saccadic overshoot.** Panel (a) shows simulated eye position for an accurate saccade (dashed black trace) and a saccade that overshoots the target (solid blue trace). When catch-up saccades made in the direction of target motion overshoot by modest amplitudes, the system (real and simulated) does not compensate by a reverse saccade, which would reduce visibility. Instead, it compensates by reducing SPEM velocity (panel (b), solid blue trace), and thus *pursuit gain*, the ratio of eye to target velocity. This relative slowing of the eye allows the target to catch up. The interval from  $t=800$  to  $t=1700$  shows the period in which the pursuit gain is reduced, with foveation occurring at  $t=1700$ . In the model, gain reduction cannot be explained by the depth of OPN pausing (panel (c)), nor by the saccade-related activity in SC (panel (d)). But a clear difference between the two episodes is apparent in two sites, MSTv (panel (e); the dashed line is the activity of MSTv cell in the opposite hemisphere in the overshoot episode) and DLPN (panel (f)), that are excited by area MT. Panel (g): In area MT, an overshoot, an accurate saccade, and an undershoot respectively entail recruitment of (relatively) low, medium, and high numbers of area MT cells in the controlling hemisphere. These recruitment levels lead to corresponding pursuit gains, in the immediate postsaccadic interval, of  $1 - \epsilon$ ,  $\sim 1$ , and  $1 + \epsilon$ , where  $\epsilon$  is a small fraction of 1. For these simulations, the initial target jump was always  $4^\circ$  right and target ramp speed was always at  $20^\circ/\text{s}$  in rightward direction

*Simulation 4: Gap effect in saccade latency.* If during pursuit, the target blinks or disappears for a short duration and then re-appears at a different location, the latency of the saccade to such a target is less than the latency of a saccade to a target that remained visible until making a similar jump (Krauzlis and Miles, 1996a; Tanaka et al., 1998). This phenomenon is similar to the reduction in latency of saccades to stationary targets seen in gap tasks (Klingstone and Klein, 1991; Tam and Stelmach, 1993), in which a foveated fixation point disappears prior to presentation of a peripheral target.

In the model, gap and blink affects on saccade latency depend primarily on inhibition of the saccadic output channel at two stages: the SC and the EBN (see Figure 1). Saccade-generating cells in the caudal SC of the model (Figure 2) receive inhibition from two sets of cells assumed to be excited while a foveated stimulus is on: fixation-activated cells in rostral SC (rSC) and fixation-activated cells in the Substantia Nigra Pars Reticulata (SNr). During gap or blink intervals, there is no visual input to such fixation-activated cells, so inhibition to caudal SC from both rSC and SNr drops, and this enables shorter saccadic latencies once the target appears and excites SC buildup and burst cells. Moreover, EBNs in the saccade generator (see Figure 1b) are normally inhibited by OPNs that, in turn, are excited by fixation-activated rSC cells. Upon disappearance of a fixation stimulus, this inhibition decreases and promotes shorter latencies. The model simulation is shown in Figure 7.

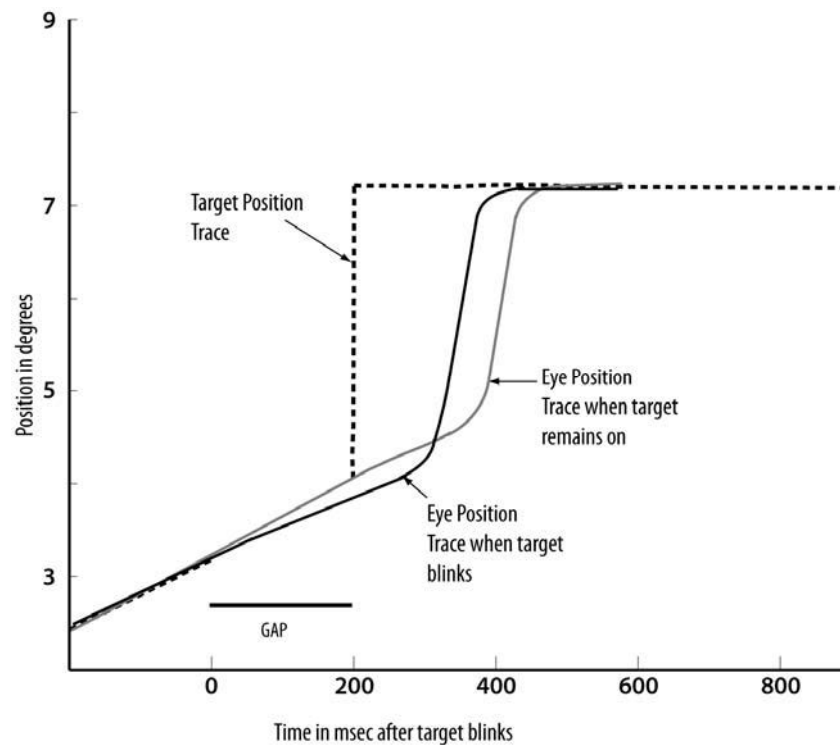


**Figure 7. Simulated gap effect on saccadic latency.** Blinking or masking of a smoothly pursued target before a step of target position reduces the latency of the saccade generated immediately after the step. This effect can be seen irrespective of prior target motion, i.e., if a stationary or moving foveated target is switched off before the onset of a stepped target, saccadic latencies are shorter than if the foveated target had remained on. The figure plots positions versus time and superposes results from two simulations. The dotted black line shows the target presentation trace, which begins with a ramp and may or may not have a gap, in display of the ramp motion, just before the step to a new, final position. For the case with a gap, the simulated eye position (solid black trace) shows a reduction in pursuit velocity during the gap, followed by a short-latency saccade in response to reappearance of the target at the

new location. When there is no gap, the eye position (thick gray trace) shows a long-latency saccade in response to the step. To simulate these conditions, ramp velocity of 20 °/s in rightward direction was used. Target was blinked for around 100ms after which, the target appears and remains stationary at 3° ahead of the current target position

*Simulation 5: SPEM direction affects the size of saccade.* Consider a catch-up saccade during pursuit. Since the target is moving, the actual position of the target at the end of the saccade will have changed from the position when the saccade was initiated. To compensate for target motion, the amplitude of a catch-up saccade typically differs from that of a saccade to a static target at the same initial eccentricity (de Brouwer, Missal et al., 2002; Eggert, Guan, Bayer, & Buttner, 2005; Guan, Eggert, Bayer, & Buttner, 2005). The saccadic system appears to use target velocity information to calibrate the amplitude of the catch-up saccade. After establishing that SC firing specified *equivalent* amplitudes for two saccades of *unequal* amplitudes made to a moving or to a stationary target, Keller, Gandhi and Weir (1996) hypothesized that the trans-SC path (SC to PPRF, Figure 1b), which programs a saccade solely on the basis of the pre-saccadic gaze-position error, is assisted by another path that corrects the programmed saccade by using information about the speed of the moving target.

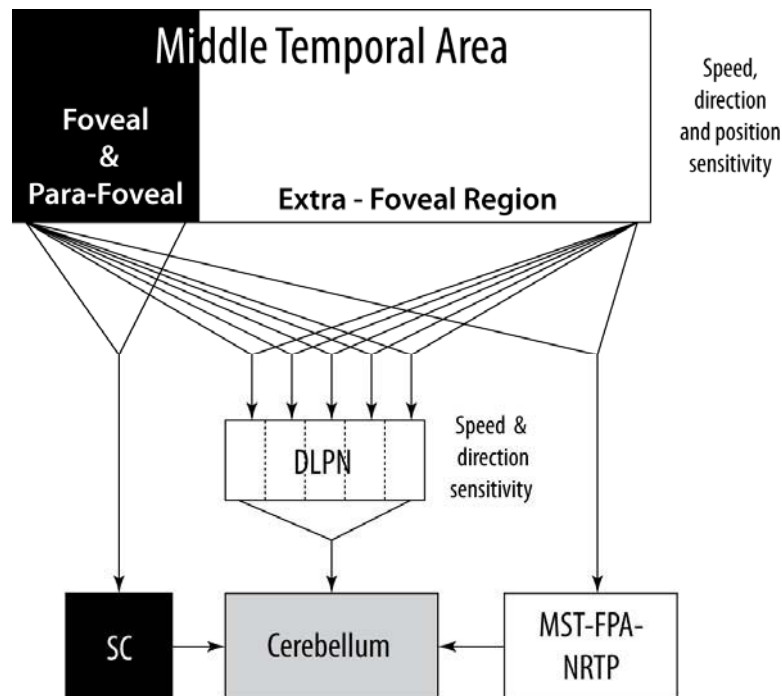


**Figure 8. Adjusting the amplitudes of saccades made to moving targets.** Cortical area MT helps inhibit small saccades and calibrate catch-up saccades. Direction-sensitive MT cells representing the foveal and parafoveal space send projections to rostral SC, thereby inhibiting small saccades. Extra-foveal MT neurons that are speed, direction and retinal-position specific project to cerebellum via DLPN (dorso-lateral pontine nucleus) cells that are speed and direction (but not retinal-position) selective. This motion vector information helps the saccadic system compensate for the target motion that occurs during a saccade by modulating the size of that saccade

In the model, speed-tuned extra-foveal MT cells project to the cerebellum via DLPN (Figure 1a), and error-guided cerebellar learning across trials converges to the correct gain for relating saccadic size increments to target velocity. The pre-saccadic gaze error causes activation of the vector error map in SC. This initiates a saccade of a particular size. In addition, velocity information from MT extra-foveal cells is processed by the cerebellum into centri-fugal or

centri-petal motions to correct saccadic size. Saccades to targets with centrifugal motion are stretched and saccades to targets with centripetal motion are shortened, thereby ensuring low position error at saccade termination.

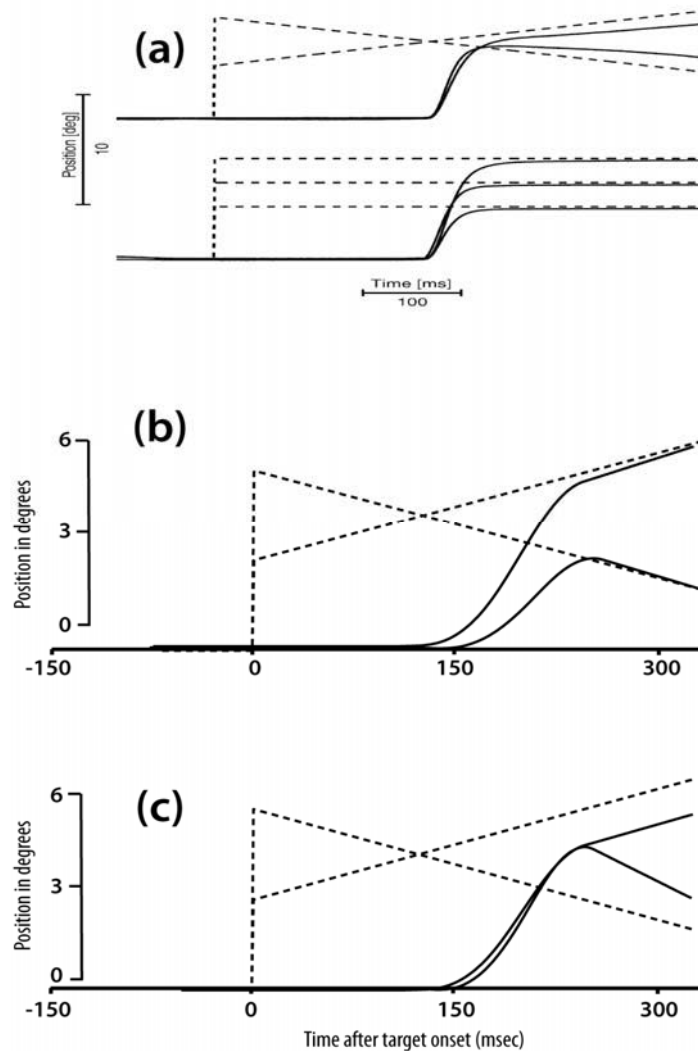


**Figure 9. Data and model simulations showing that catch-up saccades compensate for target velocity.** Amplitudes of catch-up saccades pre-compensate for a target's expected displacement due to its continued motion during the saccade. The first panel (a) shows stimuli and eye movement data from Guan et al. (2005). The second (panel (b)) and third (panel (c)) panels show simulation results with and without cerebellar compensation. In the two simulation trials, a large or a medium step occurs. The large step ( $6^\circ$ ) is followed by motion back toward the initial position (speed is  $20^\circ/s$ , towards the fixation point). The small step ( $3^\circ$ ) is followed by further motion away from the initial position (speed is  $20^\circ/s$ , away from fixation point). That the saccade in response to the larger step is notably smaller than the saccade in response to the small step in the middle panel (panel (b)) shows that the full model system (like the real system of panel (a)) is making the compensation for target velocity that is needed to improve the likelihood of having the eye fall wherever the moving target will be at the end of the saccade. The lower panel (panel (c)) shows that the model without the cerebellar component is unable to use target-motion information to pre-compensate

Figure 8 schematizes these two pathways, and Figure 9 compares data (Guan et al., 2005) with model simulations for two step-ramp stimuli. In one, the initial step is larger, but the ramp has negative slope, corresponding to target motion back toward the initial line of gaze. In the second

(presented separately but superimposed on the same plot to facilitate comparison), the initial step is smaller, but the ramp is positive, corresponding to continued motion away from the initial line of gaze. After 200 ms, the two ramp target motions reach the same point in space and cross over. The saccade to the larger step is smaller than the saccade to the smaller step, quite contrary to what one would expect if the saccade amplitudes reflected only the initial steps, but illustrative of significant velocity-based compensation. The same kind of compensation is visible in simulations of the full model (Figure 9b), but not in a model lacking learned cerebellar compensation (Figure 9c).

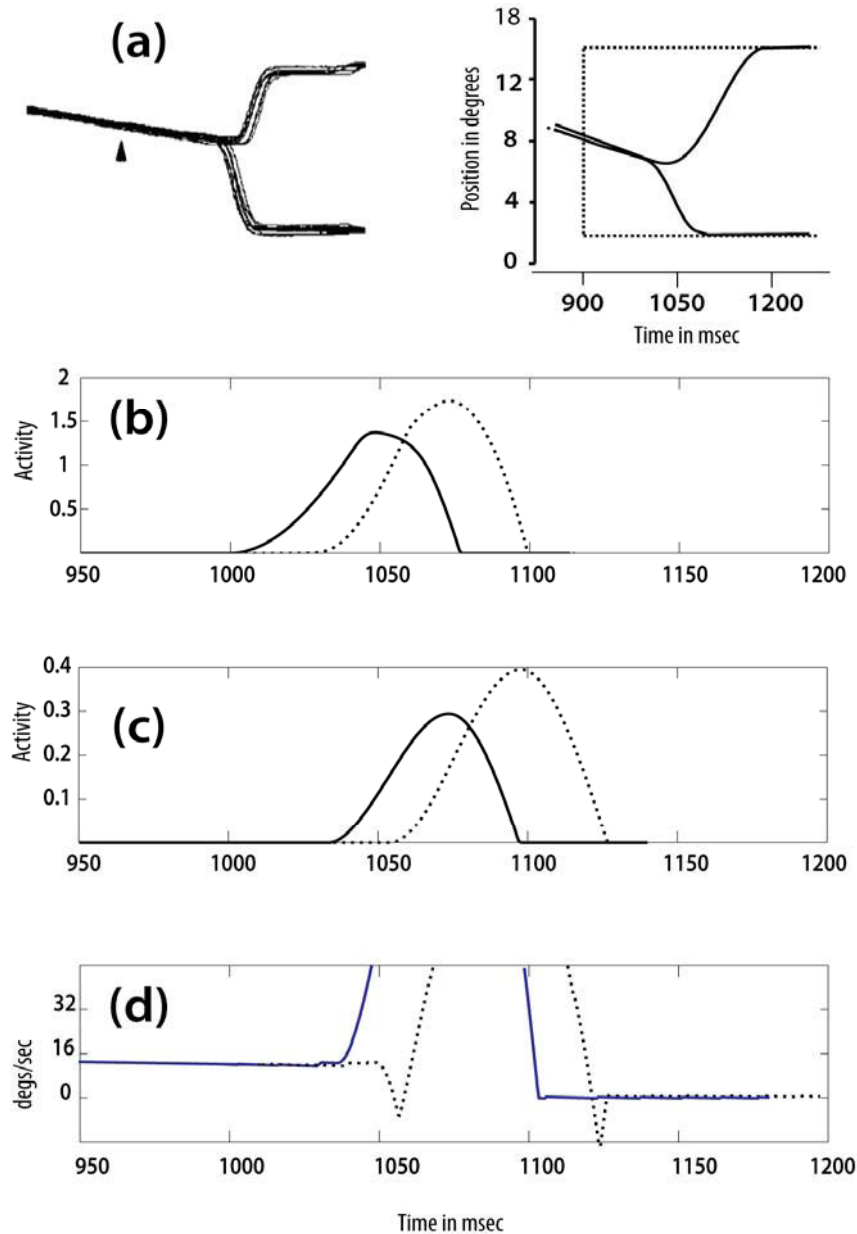


**Figure 10. Saccadic latency is affected by the direction of the target jump.** Saccades to target jumps along the direction of pursuit have smaller latencies than those to jumps opposite to the direction of pursuit. Panel (a): Left column shows data from Tanaka et al. (1998). There is a 36 ms difference between the saccadic initiation times. The right column shows results of simulations (ramp speed before step jump was 20°/s leftwards. A step jump of 6°

either direction was introduced. The target remains stationary afterwards), which yielded roughly a 25 ms difference between saccadic initiation times for saccades to jumps along, versus in the opposite direction of, target motion. The dashed trace shows the target position. Panels (b), (c) and (d) compare the activations of model LLBNs, EBNs and eye velocity traces during forward (target jump along the direction of motion) and backward saccades (jump direction is opposite to target motion) respectively. Dotted lines represent the traces for the backward saccade and thick lines illustrate the traces for the forward saccade. These panels show activity for the duration between 50 ms to 300 ms after the target jump. This time period was highlighted to exemplify the differential pontine neuronal activations that lead to forward and backward saccades. Model LLBNs and EBNs show earlier activations for the forward saccade than for the backward saccade

*Simulation 6: SPEM direction affects the latency of saccade.* Saccades to target steps in the same direction as the preceding pursuit have shorter latencies than those to target steps in the opposite direction. This asymmetry was observed in both gap and non-gap trials (Krauzlis & Miles, 1996b; Tanaka et al., 1998). Because the presence or absence of a gap makes no difference, and both steps are away from the fovea, differential OPN excitation should not be a factor. The longer time needed for the moving eye to reverse its direction is partly biomechanical: an interval of force integration is needed to slow the eye to a zero velocity. In the model, a distinct component of latency arises from the same mechanisms of velocity-dependent saccade pre-compensation just discussed. The left column of Figure 10a shows the behavioral data (Tanaka et al., 1998) and right column shows the simulation results. The target jumps at the same time and by the same amount in either of the directions (forward or backward), but in data and model the saccades made to steps in the opposite direction of SPEM take longer to initiate. The latency difference is already apparent at the EBN stage (Figures 1b and 10c), which reflects the different signals emerging from the LLBNs in the two cases. The LLBN signals (Figure 10b) differ because of the velocity dependent pre-compensation via the DLPN-CBM-LLBN pathway (Figure 1). Data from Tanaka et al. (1998) show that there is a 36 ms latency difference between forward and backward saccades. Our simulations generated a 25 ms latency difference. The extra 10 ms difference might be due to biomechanics, or switching of attention from one hemisphere to other. Human psycho-physical data (Van Donkelaar & Drew, 2002) show that attention during pursuit is either on the pursued target or ahead of it. So, for a forward saccade, the attentional resources of the same hemisphere are needed. But, for a backward saccade, the attentional resources of the opposite hemisphere should be utilized.

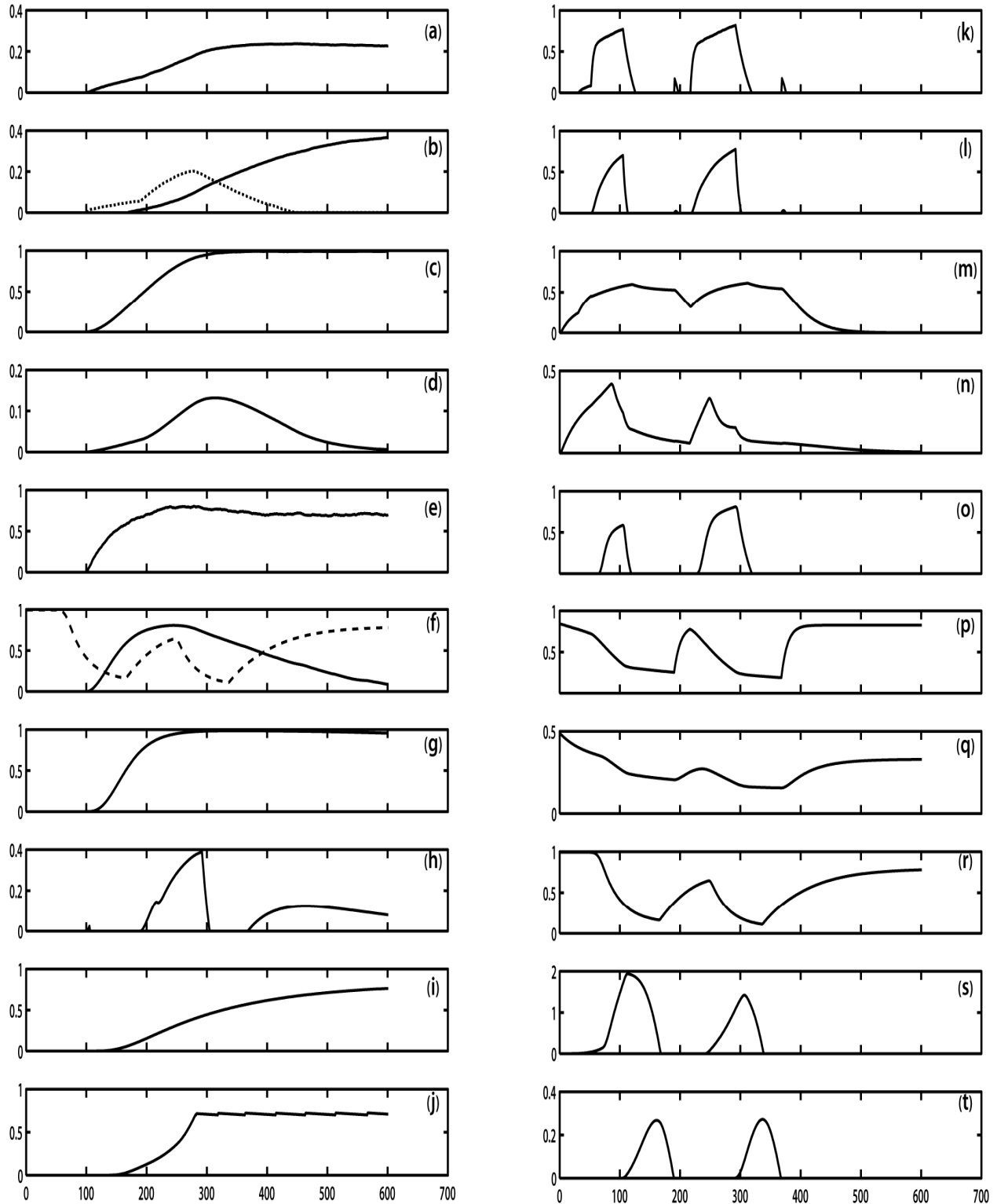


**Figure 11. Simulated activities of all the main model cell types.** The right column shows SAC system activations, the left column SPEM system activations. These simulated neural activities generated the simulated gaze behavior shown in panel (c) in the right column of Figure 5. The target stepped 4 deg rightward along the horizontal axis, and then, after a 150 ms delay, continued smooth rightward motion at a speed of 20 deg/sec. For those left-column areas where cell types are direction-selective, the plots show only activities of cells whose preferred direction aligned with

the rightward target motion direction. (a):  $MST_v$  cell; (b):  $MST_d$  cell activities for target-motion direction (dashed trace) and for background motion direction (solid trace); (c):  $FPA_i$  cell; (d):  $FPA_o$  cell; (e):  $FPA_s$  cell; (f):  $NRTP_a$  cell, with dashed overlay of OPN activity trace from (r); (g):  $NRTP_v$  cell; (h):  $DLPN$  cell; (i)  $CBM$  cell; (j):  $MVN$  cell. Right column: panels (k), (l), (m), (n) and (o), respectively, shows activities of  $FEF_v$ ,  $FEF_m$ ,  $LIP$ ,  $SC_{burst}$ ,  $SC_{buildup}$  cells whose receptive fields are centered at a 4 deg eccentricity. Panels (p), (q) and (r), respectively, represent activities of model  $FEF_{fix}$ ,  $SC_{fix}$  and OPN cells. Panels (s) and (t) show activities of  $LLBNs$  and  $EBNs$  that generate rightward eye motion

*Illustrations of simulated activation profiles for all major neuron types:* Figure 11 columns illustrate the model neural activations along the saccadic (right column) and SPEM (left column) pathways that generated the simulated gaze behaviors shown in the right column of Figure 5c. In the bottom row are shown the model neurons that send movement commands to the tonic neurons: SPEM system  $rLVN/MVN$  neurons (Figure 11j) and SAC system  $EBNs$  (Figure 11t). Because the SPEM command (Figure 11j) is zero before the first EBN burst (Figure 11t), but grows significantly during that burst, the SPEM velocity is zero before the first saccade, yet significantly positive as soon as the first saccade ends. Figure 11r shows that the OPNs, which tonically inhibit both command pathways, pause during SPEM or SAC, but much more deeply during SAC. This deep pause enables the  $EBNs$  to burst, but also permits rapid growth of the SPEM velocity command during SAC, and thus “post-saccadic enhancement”.

To illustrate this interaction, the OPN trace from Figure 11r is replotted as a dashed trace in Figure 11f, in which the continuous trace shows a model  $NRTP$  acceleration cell. The panel below it shows a model  $NRTP$  velocity cell. It is easy to see that the minimum value of OPN activity (during SAC) slightly leads the maximal acceleration toward the peak sustained SPEM velocity. Finally, the Figure also illustrates that model  $MST_v$  activity (Figure 11a) persists during sustained SPEM despite the fact that target-related model  $MST_d$  activity (Figure 11b, dashed trace) wanes as eye velocity matches target velocity, and thereby cancels target-related retinal slip, even as background slip (Figure 11b, solid trace) opposite to target direction is maintained.

## Discussion and conclusions

This article describes a neural model of how smooth pursuit and saccadic controllers interact during a variety of oculomotor tasks. The model provides a unified explanation of many recent single neuron recordings and key behavioral trends observed under various experimental conditions (e.g., de Brouwer, Missal et al., 2002; de Brouwer et al., 2001; de Brouwer, Yuksel et al., 2002; Krauzlis & Miles, 1996a, 1996b; Missal, Coimbra, Lefevre, & Olivier, 2002; Missal & Keller, 2002; Tanaka et al., 1998).

The model provides mathematically explicit answers to several fundamental questions. To the question of what happens to smooth pursuit commands when a saccade is initiated to a moving target, it answers that the two systems operate in parallel during the saccade. Such operation is feasible because the representation of target velocity computed by the model is robust in the face of the loss or degradation of target-related visual inputs, such as occurs during a catch-up saccade, but as also occurs during brief occlusions of a tracked target, and also as a normal consequence of successful SPEM, which zeros target motion, but not background motion, in the retinal frame. The assumption of parallel operation, combined with the shared omni-pauser stage, enables the model to explain post-saccadic enhancement of SPEM.

To the question of how saccades to moving targets are accurate, the model offers a two-part answer. Parallel operation means that the saccade does not have to pre-compensate for target motion to the (large) extent that it would if the SPEM system were quiescent during the saccade. However, because of underestimates of target velocity within the SPEM system in the often brief

pre-saccadic interval, or because of velocity saturation in the SPEM system, occasions regularly arise in which a catch-up saccade will be inaccurate (before learning) *despite* parallel operation of SPEM. The resulting post-saccadic foveation errors cause the cerebellar component of the model's saccadic system to learn to use target velocity information to improve the metrics of catch-up saccades. This enables the model to treat evidence for motion-based adjustments of saccade metrics as indicative of a secondary input, in addition to the positional gaze error, for saccades that are accurate despite continued target motion during the saccade.

Because saccades do degrade vision, it is also important to understand what mechanisms collectively reduce saccadic “chatter” (excessive corrective saccades) during near-accurate tracking. The model has two mechanisms that cooperate to achieve this result. Small foveation errors activate a pathway that includes MT, rostral SC and the OPNs, whose excitation inhibits saccades. Another pathway, from MT to the pons, enables a transient reduction of SPEM gain after an overshooting saccade. This reduces the need for back-tracking saccades by slowing SPEM and allowing the target to catch up with the moving line of gaze.

Two other pertinent models have recently appeared. The oculomotor control system (OCS) model (Lee & Galiana, 2005) treats symmetric control of two cameras mounted on a robotic head, and addresses how to track a moving target. The model was tested for ramp and sinusoidal trajectories, but not for a wide range of step-ramp stimuli (Rashbass, 1961). The OCS model exhibits saccade size adaptation for moving targets. Notably, it uses slip information to correct the amplitude of saccades made to moving targets. The model estimates the corrective displacement by multiplying the target's pre-saccadic retinal slip by a constant (proportional to saccadic duration) and adds it to the retinal-position error to program a compensatory saccade. However, these corrections must be quite large, because the OCS model's saccadic system effectively shuts off its smooth pursuit system during a saccadic suppression phase. Thus it cannot benefit from parallel operation of SPEM during its saccades. This causes an increase in gaze position and velocity errors after saccades (Figure 4 in Lee & Galiana, 2005). Moreover, data of Lisberger (1998) strongly suggest that the two systems do operate in parallel, as in the model we have proposed. Finally, the authors acknowledge the inability of the OCS model to explain post-saccadic enhancement of eye velocity.

Although they did not introduce a computational model, Blohm et al. (2006) proposed that a subsystem may be needed that integrates SPEM velocity commands in order to compute the SPEM-based gaze displacements needed for correct targeting of memory-guided saccades. The “smooth double-step” paradigm (McKenzie & Lisberger, 1986) analyzed by Blohm et al. (2006) uses a brief flash to specify a second saccadic target while the subject is still actively pursuing the first. Once the pursued target disappears, the subject must make a saccade to the remembered location of the briefly flashed target. Since SPEM continues up to the time of the saccade to the remembered target, that target's initially recorded retinotopic position is inaccurate by an amount equal to the integral of the post-flash SPEM velocity; i.e., the net eye-displacement since the flash. Experimental data (Blohm, Missal, & Lefevre, 2003, 2005; Gellman & Fletcher, 1992; McKenzie & Lisberger, 1986) show a range of memory-saccade latencies, and that short latency saccades are inaccurate, whereas longer latency saccades are accurate. Blohm et al., (2006) posit that only the longer latency saccades take into account the post-flash SPEM displacement. Thus, their conceptual model's saccadic pathway gets a smooth eye velocity displacement signal ( $SED_{est}$ ) generated by an eye velocity integration (EV) mechanism. Once the second target flashes, the EV mechanism starts integrating. Since the integration process is assumed to be slow, longer latencies give the saccade generator access to

better  $SED_{est}$  values, and so the ensuing saccades are accurate. The conceptual model has no specific mechanism for triggering a saccade. It uses experimental data directly as its basis for a distribution of saccadic latencies.

It seems premature to assume that the system solves problems of the type posed by such double-step experiments in the manner proposed. For example, suppose that subjects instead adopt the strategy of immediately recoding the flashed target's location from retinotopic to head-centered coordinates (cf., Grossberg & Kuperstein, 1989). Then the need to compute the intervening SPEM displacement would be obviated (if the head remains fixed, as it must if SPEM integration would be sufficient). Instead, the subject could merely compare eye position at the end of SPEM with the stored target position to compute the correct saccade vector. If this account is correct, then the fast-inaccurate saccades must be given a different explanation than lack of access to a slowly arriving displacement signal. One possibility is that the fast-inaccurate saccades actually reflect an average between two computed saccade vectors, one based on a head-centered representation and one on a not-yet-faded retinotopic representation. Such a possibility warrants examination, because in other double-flash paradigms, the probability of saccadic averaging is a declining function of saccade latency (Chou, Sommer, & Schiller, 1999). Resolving such issues is beyond the scope of the present model.

## Appendix: Model Equations and Parameters

The model is designed to capture key aspects of the processing of visual and motor signals in saccadic and smooth pursuit areas. The model simulates cell responses in such areas (Figure 1) through the use of nonlinear differential equations based on the classical membrane equation (Grossberg, 1973, 1982; Hodgkin, 1964). The system of equations was numerically integrated using the fourth order Runge-Kutta method, with a fixed step size of 0.001.

*Visual Inputs.* Each visual input to the smooth pursuit circuit is a vector field that describes the speed of the motion at each point  $(x, y)$ . The values of  $x$  and  $y$  are each constrained to be between  $[-1, 1]$  which is mapped to  $[-60^\circ, 60^\circ]$  in visual space. The velocities  $v(x, y)$  are constrained between the values  $[0, 1]$ . The target is a square block of length and width  $r$  moving in any one of the eight cardinal directions in the visual field. The center of the object is given by  $(x_0, y_0)$  and its speed is  $v_0$ . The retinal image velocity,  $v'(x, y)$ , is calculated as the difference between object speed and the eye speed at that point. Target visibility is controlled by two variables  $T_{\text{on}}$  and  $T_{\text{off}}$ , which specify the on and off times of the target in the simulation. Fixation offset is marked by  $T_{\text{fix}}$  set equal to 500.

*MT Cell.* The cells representing the input for the smooth pursuit circuit are modeled after cells found in the middle temporal area (MT). MT cells have speed and direction tuning (Maunsell & Van Essen, 1983). Two different types of cells have been observed in MT. One type,  $MT^-$  cells, respond vigorously to small stimuli moving in their receptive field at a particular speed and in a particular direction. The second type,  $MT^+$  cells, respond to large stimulus sizes. There is a large MT projection to MST. MST also has two major cell types. Cells in ventral MST ( $MST_V$ ) show direction-sensitive modulation to object motion (Tanaka, Sugita, Moriya, & Saito, 1993). Cells found in dorsal MST ( $MST_D$ ) respond to large field stimulus motion. These target tracking and navigation cells are computed using complementary subtractive vs additive operations (Grossberg, 2000; Grossberg, Mingolla, & Pack, 1999; Pack, Grossberg, & Mingolla, 2001).

We simulated 100 model MT cells for each of the eight cardinal directions (800 cells total). Each cell had a preferred speed and direction. The receptive field  $(i, j)$  was constrained to be between  $[-1, 1]$ . The speed tuning of a cell at position  $(i, j)$  is defined by a Gaussian function,  $G_{ijxy}^v$ , centered on a preferred speed  $v_{ij}$ . The direction tuning was also a Gaussian function,  $G_{ij}^d$ , centered on the preferred direction  $d_{ij}$ .

Each MT cell has a receptive field size dictated by the eccentricity of the cell from the fovea. Cells that are farther from the fovea have bigger receptive fields in keeping with the cortical magnification factor. The width of each receptive field,  $W_{ij}$ , as a function of the cell's position in retinotopic space, is given by

$$W_{ij} = \frac{25}{0.91(i^2 + j^2)^{0.5} + 1.0}. \quad (1)$$

Each MT cell has a preferred direction which is selected at random from any of the eight cardinal directions. It also has a preferred velocity,  $v_{ij}$ , chosen from the distribution  $e^{-Q(v-0.5)^2}$ . Only inputs matching these directional preferences activate the cell. For each MT cell, the total response to a motion stimulus was characterized in terms of center-surround inputs to that MT cell. The on-center response,  $\alpha_{ij}^+$ , of the receptive field to a visual target depends on the presence of three factors: the position  $(x, y)$  of the target within its receptive field, the velocity  $(v(x,y))$  of the target near the preferred velocity  $(v_{ij})$ , and the direction  $(d)$  of the target along or near the preferred direction  $(d_{ij})$  of the cell, namely:

$$\alpha_{ij}^+(v_{ij}, d_{ij}) = \sum_{x,y} G_{ijxy}^{cp} G_{ijxy}^v G_{ij}^d. \quad (2)$$

In (2),  $G_{ijxy}^{cp}$  represents the position sensitivity of the cell. It decreases as the target moves away from the center of the MT response field by:

$$G_{ijxy}^{cp} = e^{-W_y[(i-x)^2+(j-y)^2]}. \quad (3)$$

Similar to position sensitivity,  $G_{ijxy}^v$  represents the velocity tuning of the MT cell. This term reaches its maximal value if the velocity of the target ( $v(x,y)$ ) is the same as the preferred velocity ( $v_{ij}$ ) of the cell:

$$G_{ijxy}^v = e^{-G_1(v_{ij}-v(x,y))^2}. \quad (4)$$

MT cell activity also depends on the direction ( $d$ ) of target motion relative to the cells preferred direction ( $d_{ij}$ ). This term can be calculated as:

$$G_{ij}^d = e^{-G_2(d_{ij}-d)^2}. \quad (5)$$

Parameters  $G_1$  and  $G_2$ , in equations (4) and (5) equal 10 and 6, respectively.

MT cells also receive input from surround regions  $\alpha_{ij}^-$ , chosen to be five times the size of the on-centers:

$$\alpha_{ij}^-(v_{ij}, d_{ij}) = \sum_{x,y} G_{ijxy}^{sp} G_{ijxy}^v G_{ij}^d. \quad (6)$$

In (6), the position sensitivity ( $G_{ijxy}^{sp}$ ) is calculated as

$$G_{ijxy}^{sp} = e^{-\frac{W_y[(i-x)^2+(j-y)^2]}{25}}, \quad (7)$$

and  $G_{ijxy}^v$  and  $G_{ij}^d$  are defined as in equations (4) and (5).

The model computes  $MT^+$  cell activities by *adding* the surround to the center component, and  $MT^-$  cells by *subtracting* the surround from the center component.

*Subtractive Cells ( $MT^-$ )*. A model  $MT^-$  cell input is given by:

$$\beta_{ij}^-(v_{ij}, d_{ij}) = [\alpha_{ij}^+(v_{ij}, d_{ij}) - \alpha_{ij}^-(v_{ij}, d_{ij})]^+, \quad (8)$$

and its activation dynamics are described by:

$$\frac{dm_{ijvd}^-}{dt} = -m_{ijvd}^- + (1 - m_{ijvd}^-)(\beta_{ij}^-(v_{ij}, d_{ij}))(1 + [s_d^-]^+) + \sum_{ab} a_{ab} W_{abij} - (1 + m_{ijvd}^-) \sum_{e \neq d} s_e^-. \quad (9)$$

Apart from the directional tuned input ( $\beta_{ij}^-(v_{ij}, d_{ij})$ ), model  $MT^-$  also receives top-down modulatory excitatory input from the  $MST_V$  cell (term  $s_d^-$ ) having the same directional preference as the  $MT^-$  cell and from LIP (term  $\sum_{ab} a_{ab} W_{abij}$ ). It is also inhibited by  $MST_V$  cells tuned to different directions (term  $\sum_{e \neq d} s_e^-$ ) as part of the top-down attentional  $MST_V$  feedback.

Term  $\sum_{ab} a_{ab} W_{abij}$  in equation (9) and (12) represents an excitatory input from an LIP neuron with a retinotopic receptive field ( $W_{abij}$ ) that is in register with that of the recipient MT neuron:

$$W_{abij} = \begin{cases} 1 & \text{if } a - \delta/2 < i < a + \delta/2 \text{ and } b - \delta/2 < j < b + \delta/2 \\ 0 & \text{otherwise} \end{cases}. \quad (10)$$

In (10),  $\delta$  represents the diameter of LIP neurons response field. Thus,  $\sum_{ab} a_{ab} W_{abij}$  enables a saccadic decision to enhance MT and MST processing of a selected target.

*Additive Cells (MT<sup>+</sup>)*. A model MT<sup>+</sup> cell's net center-surround input is given by:

$$\beta_{ij}^+(v_{ij}, d_{ij}) = \alpha_{ij}^+(v_{ij}, d_{ij}) + \alpha_{ij}^-(v_{ij}, d_{ij}), \quad (11)$$

and its activation dynamics are described by

$$\frac{dm_{ijvd}^+}{dt} = -m_{ijvd}^+ + (1 - m_{ijvd}^+) (\beta_{ij}^+(v_{ij}, d_{ij}) (1 + [s_d^+]^+) + \sum_{ab} a_{ab} W_{abij}) - (1 + m_{ijvd}^+) \sum_{e \neq d} s_e^+. \quad (12)$$

MT<sup>+</sup> cells also receive excitatory input from MST cells, but from the dorsal sub-region (term  $s_d^+$ ) as compared to the ventral sub-region for MT<sup>-</sup> cells. They also receive an excitatory input from LIP (term  $\sum_{ab} a_{ab} W_{abij}$ ), as well as inhibition ( $-\sum_{e \neq d} s_e^+$ ), from MT<sup>-</sup> recipient MST<sub>D</sub> cells coding for non-matching directions.

The top-down inputs from MST to MT are consistent with data (Seidemann & Newsome, 1999; Treue & Maunsell, 1999) indicating that MT cell activity is modulated by top-down attention. This top-down modulatory on-center, off-surround circuit has been shown capable of focusing attention while also stabilizing learning in the network (Carpenter & Grossberg, 1993; Grossberg, 1980; Grossberg, 2003).

*MST Cells*. Inputs from model MT cells with varying speed selectivities but similar directional preferences are pooled by direction-tuned, speed-sensitive cells in the model MST. MT<sup>-</sup> cells project to MST<sub>V</sub> and MT<sup>+</sup> cells project to MST<sub>D</sub>. The MST<sub>D</sub> activities are symbolized by  $s_d^+$ , and the MST<sub>V</sub> activities by  $s_d^-$ , where subscript  $d$  indicates the cell's direction preference and  $D$  indicates direction anti-parallel to cell's preferred direction. Direction “ $d$ ” takes the values 0°, 45°, 90°, 135°, 180°, 225°, 270°, 315°.

*Target tracking Cells (MST<sub>V</sub>)*. Target tracking cells in MST ( $s_d^-$ ) calculate an estimate of predicted target velocity during pursuit. Their input comes from retinal sources (from MT) and extra-retinal sources (via a corollary discharge) and thus can provide a reliable estimate of target velocity even during sustained pursuit. The activities of the small-field MST<sub>V</sub> cells are given by:

$$\frac{ds_d^-}{dt} = -s_d^- + (1 - s_d^-) [2.5 \sum_{ij} [m_{ijvd}^-]^+ v_{ij} + 5.5 [s_D^+]^+ + 2(k_d - k_D)]^+ - 75 \sum_{e \neq d} s_e^-. \quad (13)$$

In (13), term  $\sum_{ij} m_{ijvd}^- v_{ij}$  gives an estimate of the average velocity computed by the MT<sup>-</sup> cells having the same direction preference. Other sources of excitatory input come from the large-field MST<sub>D</sub> cell having an opposite direction to this MST<sub>V</sub> cell (term  $s_D^+$ ), and via corollary discharge ( $k_d - k_D$ ) (see Pack et. al. (2001)). There is also mutual inhibition between the MST<sub>V</sub> cells coding other directions (term  $-75 \sum_{e \neq d} s_e^-$ ).

Input from MST<sub>D</sub> cell having an opposite direction to MST<sub>V</sub> cell that represents a pursued target to be excited by the background counter-motion generated by SPEM. Such excitation helps MST<sub>V</sub> to better compute predicted target velocity when visual motion inputs

decrease from  $MT^-$  cells to  $MST_V$  cells during successful pursuit. In equation (13),  $k_d$  is a corollary discharge, or efference copy, from the pursuit neurons of the vestibular nucleus that fire when the eye moves in direction  $d$  (see equation (26) below), and  $k_D$  is the corollary discharge from pursuit neurons that fire when the eye moves in the direction  $D$  that is opposite to  $d$ . Term  $k_d$  is calculated as a mix of the two nearest orthogonal signals  $\theta$  and  $\theta + 90^\circ$  to  $d$  from the values  $0^\circ, 90^\circ, 180^\circ$  and  $270^\circ$  :

$$k_d = \sqrt{h_\theta^2 + h_{\theta+90}^2}. \quad (14)$$

These corollary discharge signals, which grow as the eye velocity grows to match the velocity of the SPEM target, can also compensate for the reduction of small-field visual motion signals that attend any successful SPEM. The result is that  $MST_V$  cells can provide a reliable estimate of predicted target velocity throughout a SPEM episode, namely before SPEM onset, during SPEM acceleration, and during steady-state matching of eye to target velocity.

Motion opponency of the efference signals ( $k_d - k_D$ ) in equation (14) supports this type of activity profile. During SPEM onset,  $[k_d - k_D]$  is zero. Once the eye starts to move,  $[k_d - k_D]$  becomes excitatory for  $MST_V$  cells aligned along direction of target motion and inhibitory for the  $MST_V$  cells in the opposite direction. This pattern is reversed for  $MST_D$  cells as seen in the equation (15).

*Navigation Cells ( $MST_D$ ).*  $MST_D$  cell get input from the large receptive field  $MT^+$  cells having same directional preference, and so is sensitive to coherent background motion. The activities of the large-field  $MST_D$  cells are given by:

$$\frac{ds_d^+}{dt} = -s_d^+ + (1 - s_d^+) [0.1 \sum_{ij} [m_{ijvd}^+] + 5.5 [s_d^-] + 2(k_D - k_d)] + -15 \sum_{e \neq d} s_e^+. \quad (15)$$

The excitatory input to  $MST_D$  cells comes from three sources:  $MT^+$  cells ( $\sum_{ij} m_{ijvd}^+$ ) having the same directional preference as the model  $MST_D$  cell, the  $MST_V$  cell ( $s_d^-$ ) having the same directional preference, and via corollary discharge ( $k_D - k_d$ ). There is mutual inhibition between the  $MST_D$  cells coding other directions (term  $-15 \sum_{e \neq d} s_e^+$ ). Note that the corollary discharge input ( $k_D - k_d$ ) to the cell is the opposite of the corollary discharge to  $MST_V$  cell (see equation (13)). This opponency ensures that, during sustained pursuit, the activity of  $MST_D$  cells tuned to background motion direction remains bounded and does not affect the current pursuit dynamics.

*FPA Cells:* The frontal pursuit area (FPA) is considered to be the first area where a sensory-to-motor transformation of SPEM signals takes place. The model FPA contains three cell types that model cells reported in literature (Tanaka & Lisberger, 2002a):

*Winner-Take-All cells (WTA).* WTA cells receive input from target-tracking cells of  $MST$  and convey this information to the target-selective FPA vector averaging cells. Their activity,  $f_d^I$ , obeys:

$$\frac{df_d^I}{dt} = -2f_d^I + (1 - f_d^I)(50[s_d^-] + 10f_d^R) - 10 \sum_{e \neq d} f_e^I. \quad (16)$$

By (16), these cells are excited by  $MST_V$  cells (term  $50s_d^-$ ) having the same directional preference, and by self excitatory interneurons (term  $10f_d^R$ ). There is mutual inhibition among

input cells with different direction preferences (term  $-10\sum_{e \neq d} f_e^I$ ). The excitatory interneurons within the input layer support self-sustaining activity:

$$\frac{df_d^R}{dt} = -f_d^R + (1 - f_d^R)[f_d^I]^+. \quad (17)$$

*Vector Summation cells.* Vector summation cells receive input from the navigation cells of MST and provide additional acceleration during pursuit initiation. These activities obey:

$$\frac{df_d^S}{dt} = -f_d^S + (1 - f_d^S)15[s_d^+]^+ - (1 + f_d^S)\sum_{e \neq d} f_e^S. \quad (18)$$

Summation cell activities ( $f_d^S$ ) are excited by MST<sub>D</sub> cells of the corresponding direction (term  $15s_d^+$ ), and have low mutual inhibition (term  $-\sum_{e \neq d} f_e^S$ ). This inhibition enables two stimulus directions to be simultaneously active and enables vector averaging to occur before target selection.

*Vector Averaging Output cells.* Model vector averaging cells perform the role of target selection cells in the SPEM system. These cells interact with basal ganglia via thalamus and help decide the target stimulus among many distractors. These activities obey:

$$\frac{df_d^O}{dt} = -10f_d^O + (1 - f_d^O)(15[f_d^I]^+ + [f_d^S]^+ + 15\mu^d + 1.5[g^P - 0.5]^+) - 25(1 + f_d^O)\sum_{e \neq d} f_e^O. \quad (19)$$

FPA output activities ( $f_d^O$ ) are excited by FPA input cells (term  $15f_d^I$ ) and summation cells ( $f_d^S$ ) having the same direction preference, by electrical stimulation ( $\mu^d$ ), and by a cortico-thalamic decision signal ( $[g^P - 0.5]^+$ ). The cortico-thalamic decision signal helps in target selection when more than one stimulus is present in the environment. The output cells receive strong inhibitory input from output cells with different direction preferences (term  $-25\sum_{e \neq d} f_e^O$ ). If several FPA input cells are active at the same time, indicating more than one moving target, the output cells show a reduced response due to this inhibitory process.

Model FPA output cells carry the estimate of target velocity. FPA WTA cells (see equation (16)) receive direct inputs from MST<sub>V</sub> cells which estimate the target velocity. This activity is sustained even during target blink via the self-excitatory interneuron. During single stimulus tracking, FPA output cells carry the target velocity estimate from MST<sub>V</sub> to NRTP. When multiple stimuli are present, FPA input cells hold the representations of all stimuli until FPA output cells decide the target among the distractors. Once FPA output cells select a target for a future SPEM, the activity of FPA input cells representing the distractor starts decaying.

*Decision signal ( $g^P$ ).* Onset of the gating signal  $g^P$  in (19) occurs once the total activity reaches 0.5. Then, BG-Thal sends a nonspecific signal that boosts the activity of all the FPA averaging cells. Mutual inhibition helps choose the winner. Thus, this interaction results in a choice that is controlled by a cortico-basal ganglia-thalamocortical loop (Basso & Wurtz, 2002; Brown et al., 2004). Its value is calculated as:

$$\frac{dg^P}{dt} = -0.2g^P + (1 - g^P)\sum_d [f_d^O - 0.33]^+. \quad (20)$$

In (20),  $g^P$  is activated by a thresholded input from FPA output cells ( $f_d^O$ ). When  $g^P$  exceeds 0.5 (see equation (19)), the FPA output cell with maximal activity is chosen as the target and the competition is silenced via strong mutual inhibition.

*Pontine nuclei.* Pontine nuclei act as way stations for the SPEM information transfer from cortex to cerebellum. We have modeled two important pontine nuclei, namely DLPN and NRTP.

*DLPN Cells.* DLPN cells have large receptive fields covering almost the whole contralateral visual field and have directional preferences and speed selectivities similar to MT cells. There is no topographic arrangement of cells in DLPN. The activities of DLPN cells obey:

$$\frac{dp_{vd}^D}{dt} = -p_{vd}^D + 0.1(1 - p_{vd}^D) \sum_{ij} [m_{ijvd}^-]^+ - 100(1 - p_{vd}^D) \sum_{\substack{e \neq d \\ f \neq v}} p_{fe}^D. \quad (21)$$

By (21), DLPN cells receive convergent excitatory inputs from all  $MT^-$  cells of the same speed and direction (term  $m_{ijvd}^-$ ). Mutual inhibition among DLPN cells (term  $-100 \sum_{\substack{e \neq d \\ f \neq v}} p_{fe}^D$ ) enables only

those neurons whose velocity tuning is close to that of the target velocity to remain active. Therefore, model DLPN cells output an approximate estimate of target velocity without regard to its specific retinotopic locus. This approximate estimate provides drive to the initial eye acceleration (see equation (24)) and helps the cerebellum make corrections to the amplitudes of saccades made to moving targets (see equation (70)).

*NRTP Cells.* Two types of pursuit-related cells have been observed in NRTP: acceleration cells and velocity cells (see Simulation 2 and Figure 4). We predict that the acceleration cells act within an internal negative feedback loop to compute the difference between estimated target velocity and eye velocity. The velocity cells integrate acceleration cell output.

*NRTP Acceleration cells:* NRTP acceleration cell output acts as a mismatch detector between the estimates of target and eye velocities. The activities of these cells obey the equation:

$$\frac{dp_{ad}^N}{dt} = -p_{ad}^N + 45(1 - p_{ad}^N) [f_d^O - k_d]^+ - 50 \sum_{e \neq d} p_{ae}^N. \quad (22)$$

The acceleration cells ( $p_{ad}^N$ ) are excited by the difference between  $f_d^O$ , the FPA output that estimates target velocity, and  $k_d$ , the vestibular nuclei (rLVN/ MVN, see equation (14)) output that controls, and thus estimates, eye velocity. There is also mutual inhibition between different NRTP acceleration cells ( $-50 \sum_{e \neq d} p_{ae}^N$ ).

*NRTP Velocity cells:* The activities of these cells follow the equation:

$$\frac{dp_{vd}^N}{dt} = -0.4 p_{vd}^N + 40(1 - p_{vd}^N) [p_{ad}^N]^+. \quad (23)$$

Acceleration cell activity  $p_{ad}^N$  in equation (22) is the only excitatory input to the velocity integrator cells.

*CBM Cells.* The model cerebellum is highly simplified. It channels sub-cortical SPEM information from NRTP and DLPN towards the vestibular nuclei which control the eye muscles. Hence, cerebellectomy results in large and lasting deficits in pursuit (Zee, Yamazaki, Butler, & Gucer, 1981). The activities of these cells are given by:

$$\frac{dc_d^P}{dt} = -0.5c_d^P + (1 - c_d^P)(10 \sum_v [p_{vd}^D]^+ + 20p_{vd}^N) - 25(1 + c_d^P) \sum_{e \neq d} c_e^P. \quad (24)$$

The cerebellum cell activities  $c_d^P$  are directionally tuned and receive excitatory input from DLPN ( $\sum_v p_{vd}^D$ ) and NRTP ( $p_{vd}^N$ ) from both hemispheres. Mutual inhibition occurs across directions ( $-25 \sum_{e \neq d} c_e^P$ ). Since cerebellum cells are velocity sensitive but not velocity tuned, the DLPN cell input is pooled over all velocities along a particular direction.

*rLVN/MVN cells.* Vestibular nuclei (medial and rostro-lateral vestibular nuclei) represent the penultimate stage of processing for SPEM. Here the directional representation is broken down from its cardinal axes into axes along which the muscle can move the eye. Since there are eight cardinal directions ( $d$ ) represented by the model cerebellar pursuit cells and there are 4 orthogonal directions in which the muscle can move the model eye (represented by  $\theta$ ), the outputs from three cerebellum cells form one rLVN/MVN input. For example, the rLVN/MVN input along the upward direction ( $\theta = 90^\circ$ ), is defined by adding the cerebellar cells that are active for top-right ( $d = 45^\circ$ ), top ( $d = 90^\circ$ ), and top-left ( $d = -45^\circ$ ) directions:

$$I_\theta^P = c_{\theta-45^\circ}^P + c_\theta^P + c_{\theta+45^\circ}^P. \quad (25)$$

Pursuit neuron activities in the rLVN/MVN are defined by:

$$\frac{dh_\theta}{dt} = -0.6h_\theta + 4I_\theta^P - 1.5I_\Theta^P - 7.5v(o). \quad (26)$$

By (26), these cells receive pursuit input ( $4I_\theta^P$ ) from the cerebellum. They are inhibited by opponent direction pursuit input ( $-1.5I_\Theta^P$ ) and by the omnipause neurons ( $-v(o)$ ) in the brain stem. The signal function  $v(x)$  is a sigmoid, calibrated such that inhibition from OPNs during pursuit is not enough to totally inhibit activity of pursuit neurons. It is given by:

$$v(x) = \frac{x^4}{x^4 + 0.5^4}. \quad (27)$$

During sustained pursuit, the inhibition from OPNs is high, but not strong enough to inhibit pursuit activity. During saccades, OPNs become silent and this causes the inhibition to become zero and helps pursuit neurons to reach the target velocity faster (post-saccadic enhancement of eye velocity, see Simulation 2). As above, direction  $\theta$  takes the values of  $0^\circ$ ,  $90^\circ$ ,  $180^\circ$  and  $270^\circ$ , which represent rightward, upward, leftward and downward directions of motion. Parameter  $\Theta$  in equation (26) is defined as:  $\Theta = \theta + 180^\circ$ .

*OPN cells.* Omnipause neurons (OPNs) are tonically active cells present in the nucleus raphe interpositus and are known to inhibit saccades. They are active during periods of sustained pursuit and fixation, but become silent during saccades. The model OPN activities follow Gancarz and Grossberg (1999) and are defined as:

$$\frac{do}{dt} = -0.2o + (1 - o)(1.2 + 20[u_{ff}]^+) - 3.5(o + 0.4)(20v(l_\theta) + 5v(h_\theta)). \quad (28)$$

Model OPNs are excited by an arousal signal (term  $1.2$ ) and SC fixation cell output (term  $u_{ff}$ , see equation (42)). These cells are inhibited by long lead burst neurons ( $v(l_\theta)$ , see equation (73)) as well as pursuit neurons ( $v(h_\theta)$ , see equation (26)), but by varying degrees. The sigmoidal signal function ( $v(x)$ ) obeys:

$$v(x) = \frac{x^4}{x^4 + 0.1^4}. \quad (29)$$

The strength of inhibition from long lead burst neurons is stronger than pursuit neurons because OPNs go silent during saccades but are active at 66% of their maximal value during maintained pursuit (Missal & Keller, 2002).

*SC Cells.* The model SC includes two cell layers or maps: SC burst cells and buildup cells (Munoz & Wurtz, 1993a, 1993b, 1995a, 1995b). SC receives collaterals from FEF, LIP and from LGN. Activities of these cells are represented by equations which are similar to equations in Gancarz and Grossberg (1999).

*SC Burst Cells.* Model SC burst cells represent the saccadic burst cells present in SC (Munoz & Wurtz, 1993a, 1993b, 1995a, 1995b). These have a burst of activity before a saccade and are quite silent during fixation and saccade preparation periods. Burst cell activities  $b_{ij}$  obey the equation:

$$\frac{db_{ij}}{dt} = -20b_{ij} + (1.2 - b_{ij})B_{ij}^E - (1 + b_{ij})B_{ij}^I, \quad (30)$$

where the excitatory input equals:

$$B_{ij}^E = 8r_{ij} + 30f(u_{ij}) + 155.0[f_{ij}^O]^+, \quad (31)$$

SC burst cells receive excitatory input from the retina ( $r_{ij}$ ), from buildup cells ( $u_{ij}$ , see equation (35)) and from the output layer of the FEF ( $f_{ij}^O$ , see equation (54)). The sigmoidal signal function ( $f(u_{ij})$ ) is defined as:

$$f(x) = \frac{x^3}{x^3 + 0.07^3}. \quad (32)$$

The SC burst cell inhibitory input equals:

$$B_{ij}^I = 10M + 70[u_{ff}]^+ + 110n(n_{ij}). \quad (33)$$

These cells are inhibited by the mesencephalic reticular formation ( $M$ , see equation (46)), the fixation cell ( $u_{ff}$ , see equation (42)) and by the substantia nigra ( $n(n_{ij})$ , see equation (47)). The sigmoidal function ( $n(x)$ ) is defined as:

$$n(x) = \frac{x^3}{x^3 + 0.4^3}. \quad (34)$$

*SC Buildup Cells.* Model buildup cells mimic the SC buildup cells in SC. They have no activity during fixation and show sustained buildup activity during the saccade preparation phase followed by a burst of activity prior to saccade initiation. The activities of the SC buildup cell layer ( $u_{ij}$ ) obey the equation:

$$\frac{du_{ij}}{dt} = -0.1u_{ij} + (1 - u_{ij})U_{ij}^E - u_{ij}U_{ij}^I. \quad (35)$$

The excitatory input to SC buildup cells ( $U_{ij}^E$ ) is given by:

$$U_{ij}^E = r_{ij} + 5[f_{ij}^I]^+ + [a_{ij}]^+ + 40c(u_{ij}) + 4 \sum_l \sum_k g(b_{lk} H_{k-j} H_{l-i}), \quad (36)$$

where

$$g(x) = 0.035x^{0.65}. \quad (37)$$

SC buildup cells are excited by the retina ( $r_{ij}$ ), the planning layer of the FEF ( $f_{ij}^I$ , see equation (48)), the parietal cortex ( $a_{ij}$ , see equation (59)), and via self-excitatory connections ( $c(u_{ij})$ ), and by the burst cell layer ( $b_{lk}$ ). The self-excitatory feedback signal is threshold-linear:

$$c(x) = [x - 0.035]^+. \quad (38)$$

The spread of input from the burst layer to buildup layer is a Gaussian described by:

$$H_i = 100e^{-i^2}. \quad (39)$$

The inhibitory input to SC buildup cells ( $U_{ij}^I$ ) is given by:

$$U_{ij}^I = 40M + 0.8[u_{ff}]^+ + 8n(n_{ij}) + \sum_{\substack{l=j-6 \\ l \neq j}}^{l=j+6} \sum_{\substack{k=i-6 \\ k \neq i}}^{k=i+6} c(u_{kl})M_{k-l}M_{l-j}. \quad (40)$$

Inhibition comes from the mesencephalic formation (term  $M$ ), the fixation cell ( $u_{ff}$ ), the substantia nigra ( $n(n_{ij})$ ), and other buildup cells ( $c(u_{kl})$ ). There is strong mutual inhibition between buildup cells. The strength ( $M_i$ ) of this inhibition is a Gaussian function of distance:

$$M_i = e^{-0.02i^2}. \quad (41)$$

*SC Fixation Cells.* Fixation cells are active during fixation and become silent during saccades. Model SC fixation cells obey:

$$\frac{du_{ff}}{dt} = -0.1u_{ff} + (0.1 - u_{ff})(10\zeta + r_{00} + K^E) - u_{ff} \left( 10 \sum_{\substack{k=1 \\ k \neq f}}^N \sum_{\substack{j=1 \\ j \neq f}}^N u_{kj} M_j M_k + 10 \sum_{\substack{k=1 \\ k \neq f}}^N \sum_{\substack{j=1 \\ j \neq f}}^N b_{kj} \right). \quad (42)$$

The fixation cell activity ( $u_{ff}$ ) is excited by a fixation signal (term  $\zeta$ ), defined as:

$$\zeta = \begin{cases} 1.0 & \text{if } t < T_{\text{fix}} \quad (T_{\text{fix}} \text{ is the time at which fixation light goes off}) \\ 0 & \text{otherwise} \end{cases}. \quad (43)$$

It is also excited by visual input from the fovea ( $r_{00}$ ) and MT cells ( $K^E$ , see simulation 1) whose receptive fields contain the fovea, defined by:

$$K^E = \sum_{ij \in F_\delta} m_{ijvd}^- \quad \text{where } F_\delta = \left\{ (i, j) \text{ such that } f - \delta \leq i \leq f + \delta \right. \\ \left. \text{and } f - \delta \leq j \leq f + \delta \right\}. \quad (44)$$

In (44),  $\delta$  is the radius of response field of the MT cell at position  $(i, j)$ , and  $f$  indicates the position of the fovea.

Activity in buildup cells (term  $u_{kj}$ ) or burst cells (term  $b_{kj}$ ) inhibits fixation cell activity. As a result, once a saccade is initiated, fixation cells go silent. Since buildup layer cells are involved in saccade planning as well as saccade execution, both buildup and fixation cell activity can co-exist. This property is realized by using a distance-dependent Gaussian inhibition from

buildup cells to fixation cells (term  $10 \sum_{k=2}^N \sum_{j=2}^N u_{kj} M_j M_k$ ). The buildup inhibitory kernel equals:

$$M_i = 0.1e^{-0.01i^2}. \quad (45)$$

*MRF Cells.* The mesencephalic reticular formation input in equations (33) and (40) is defined by:

$$M = \begin{cases} 1 & \text{if } \sum_{i, j \neq \text{fovea}}^N u_{ij} > 0 \\ 0 & \text{otherwise} \end{cases}. \quad (46)$$

It is active if there is any activity in the nonfoveal part of SC buildup cell layer ( $u_{ij}$ ).

*SNr Cell.* Cell activity ( $n_{ij}$ ) in the model substantia nigra follows the equation:

$$\frac{dn_{ij}}{dt} = (1 - n_{ij})(1.7 + 200\zeta) - 2(1 + n_{ij})n(f_{ij}^I). \quad (47)$$

It is excited by a constant arousal signal (term  $1.7$ ) and by the fixation signal ( $\zeta$ , see equation (43)). The nigral cells are inhibited by the FEF planning layer cells ( $f_{ij}^I$ , see equation (48)).

*FEF Cells:* The model's frontal eye field is comprised of two cell layers or maps: FEF planning cells and output cells.

*FEF planning layer cells.* The FEF planning layer cells are involved in saccadic planning and execution. Reciprocal connections with LIP help these cells achieve target selection in a stimulus rich environment. The equations for planning cell activity  $f_{ij}^I$  at each position ( $i, j$ ) is a simplified representation of a similar equation in Brown et al. (Brown et al., 2004):

$$\frac{df_{ij}^I}{dt} = (1 - f_{ij}^I)F_{ij}^{PE} - (f_{ij}^I + 0.4)F_{ij}^{PI}, \quad (48)$$

where the excitatory input ( $F_{ij}^{PE}$ ) obeys:

$$F_{ij}^{PE} = 10[a_{ij}]^+ + 15I_{ij} + 1.5[g^S - 0.5]^+ + 2f(f_{ij}^I). \quad (49)$$

Each planning layer cell at position ( $i, j$ ) receive excitatory input from the parietal cortex ( $a_{ij}$ ), and from a smoothed retinal input ( $I_{ij}$ ) defined as:

$$I_{ij} = \sum_{(p,q) \in \Psi} R_{ij} \exp\left(\frac{-(p-i)^2 - (q-j)^2}{0.7^2}\right), \quad (50)$$

where  $\Psi$  is the set of eight nearest neighbors in cartesian input space. Additional excitatory input in equation (49) comes from the decision variable ( $[g^S - 0.5]^+$ ) and via a self-excitatory recurrent on-center (term  $2f(f_{ij}^I)$ ). When the decision signal ( $g^S$ ) goes over 0.5, it boosts the activity of all active neurons. This additional excitation gets amplified by the self-excitatory loop. That is, this combination ensures that the maximally active neuron gets the biggest boost in activity compared to the rest of the neurons. Thus, this combination realizes a target selection network among the planning layer neurons. The sigmoidal signal function ( $f(x)$ ) controlling the FEF planning cell input is defined as:

$$f(x) = \frac{([x]^+)^8}{([x]^+)^8 + 0.5^8}. \quad (51)$$

The inhibitory input to equation (48) obeys:

$$F_{ij}^{PI} = 0.8 + 10([f_{ff}^I]^+ e^{-((i-f)^2 + (j-f)^2)}) + 20 \sum_{\substack{r \neq i \\ s \neq j}} f_{rs}^I + 10S_{on}. \quad (52)$$

In (52), each planning layer cell receives a distance-dependent inhibition from the FEF fixation cell (term  $f_{ff}^I$ ), and from other active FEF planning cells via recurrent inhibition ( $20 \sum_{\substack{r \neq i \\ s \neq j}} f_{rs}^I$ ).

These cells also get strong inhibition after saccade initiation in the form of “*saccade on*” signal ( $S_{on}$ ). This signal takes the value 1 only if a saccade is underway and is zero during the rest of the interval. This might be thought of as FEF post-saccadic cell input.

*FEF fixation cell.*  $f_{ff}^I$  is the activity of the FEF fixation cell that is analogous to the SC fixation cell. It obeys the equation:

$$\frac{df_{ff}^I}{dt} = -0.1f_{ff}^I + (1 - f_{ff}^I)(10\zeta + r_{00}) - (1 + f_{ff}^I)F_{ff}^I. \quad (53)$$

This cell receives excitatory input from the fovea ( $r_{00}$ ) and from the fixation input ( $\zeta$ , described in equation (43)). The inhibitory input to the fixation cells obeys:

$$F_{ff}^I = 0.1 \sum_{ij} (f_{ij}^I e^{-0.01((i-f)^2 + (j-f)^2)} + f_{ij}^O). \quad (54)$$

FEF fixation cells are inhibited by the FEF input cells ( $f_{ij}^I$ ) and output cells ( $f_{ij}^O$ ), much like the SC fixation cells.

*FEF Output cells.* Model FEF output cells correspond to FEF movement or presaccadic cells. They convey the saccadic choice to SC and to the saccade generator in brainstem and thereby help execute a saccade. Their activities are defined by:

$$\frac{df_{ij}^O}{dt} = (1 - f_{ij}^O)F_{ij}^{OE} - (f_{ij}^O + 0.8)F_{ij}^{OI}. \quad (55)$$

In (55), the excitatory input  $F_{ij}^{OE}$  obeys the equation:

$$F_{ij}^{OE} = 0.4[f_{ij}^I - 0.2]^+ + 5[a_{ij}]^+ + 1.5[g^S - 0.5]^+. \quad (56)$$

Excitatory inputs come from FEF input cells ( $0.4[f_{ij}^I - 0.2]^+$ ) and parietal cells ( $5a_{ij}$ ), but their suprathreshold activation strongly depends on excitation by the decision signal ( $1.5[g^S - 0.5]^+$ ).

The inhibitory input  $F_{ij}^{OI}$  in equation (55) obeys:

$$F_{ij}^{OI} = 20 \sum_{\substack{p \neq i \\ q \neq j}} f_{pq}^O, \quad (57)$$

which provides strong mutual inhibition from other FEF output cells ( $20 \sum_{\substack{p \neq i \\ q \neq j}} f_{pq}^O$ ). This strong

mutual inhibition ensures that only the maximally active cell in the planning layer goes on to become a motor output, i.e., to generate a saccade.

*Decision Signal.* The decision variable  $g^S$ , which is meant to represent the results of a competitive choice by a cortico-(basal ganglia)-thalamo-cortical loop (see in Brown et al., 2004):

$$\frac{dg^S}{dt} = -0.6g^S + 20(1 - g^S) \left( \sum_{ij} ([f_{ij}^I - 0.33]^+ + [a_{ij} - 0.6]^+ + [u_{ij} - 0.2]^+) \right). \quad (58)$$

In (58), activity  $g^S$  is maximal when there are synchronous inputs from all the three retinotopically in-register areas namely: FEF planning layer cells ( $f_{ij}^I$ ), LIP visual cells ( $a_{ij}$ ), and SC buildup cells ( $u_{ij}$ ). Higher values of  $g^S$  enable faster target selection.

*PPC Cells.* Parietal cortex cell activities ( $a_{ij}$ ) represent the responses in the lateral bank of intra-parietal area (LIP), which code visual stimuli in motor error coordinates. They receive retinal and FEF input and project back to the FEF. They are modeled as:

$$\frac{da_{ij}}{dt} = (1 - a_{ij})[I_{ij} + [f_{ij}^I]^+ + f(f_{ij}^O) + f(a_{ij})] - a_{ij}[20 \sum_{\substack{x \neq i \\ y \neq j}} [a_{xy}]^+ + a_{ij}^R]. \quad (59)$$

The excitatory input consists of a smoothed retinal input ( $I_{ij}$ , see equation (50)), FEF planning cells ( $f_{ij}^I$ ), FEF output cells ( $f(f_{ij}^O)$ ), and recurrent on-center connections ( $f(a_{ij})$ ). The parameters for the sigmoidal signal function ( $f(x)$ , in equation (59)) were chosen such that there is sustained activity even during the delay period of the delayed-saccade paradigm. It is described as:

$$f(x) = \frac{x^7}{x^7 + 0.4^7}. \quad (60)$$

The inhibitory input to these cells consists of recurrent off-surround connections ( $20 \sum_{\substack{x \neq i \\ y \neq j}} [a_{xy}]^+$ )

and a more slowly varying recurrent self-inhibition ( $a_{ij}^R$ , see equation (61)). Dynamics for the interneuron-mediated self-inhibition obey:

$$\frac{da_{ij}^R}{dt} = (1 - a_{ij}^R)a_{ij} - a_{ij}^R. \quad (61)$$

These inhibitory connections replicate the slow decay of delay-period activity observed in primate parietal cells when the animal was doing a delayed saccade.

*CBM cells:* SC burst cells ( $b_{ij}$ ) and FEF output cells ( $f_{ij}^O$ ) activate cerebellar cells that control the learning of eye movement gains. The SC-activated cerebellar cell activities ( $c_{ij}^S$ ) obey:

$$\frac{dc_{ij}^S}{dt} = -0.1c_{ij}^S + (1 - c_{ij}^S)r(b_{ij}) - 6(c_{ij}^S + 0.05) \sum_{i,j=1}^N o(c_{ij}^F). \quad (62)$$

Here, excitatory input comes from SC burst cells ( $r(b_{ij})$ ) and inhibition from all cerebellar FEF-activated cells ( $-\sum_{i,j=1}^N o(c_{ij}^F)$ ). Similarly, FEF-activated cells activities ( $c_{ij}^F$ ) obey:

$$\frac{dc_{ij}^F}{dt} = -0.1c_{ij}^F + (1 - c_{ij}^F)r(f_{ij}^O) - (c_{ij}^F + 0.05) \sum_{i,j=1}^N o(c_{ij}^S). \quad (63)$$

These cells are excited by the output layer of FEF ( $r(f_{ij}^O)$ ) and inhibited by all the cerebellar SC cells ( $-\sum_{i,j=1}^N o(c_{ij}^S)$ ). The SC and FEF cerebellar cells hereby inhibit each other and compete for dominance (Gancarz and Grossberg, 1999). The excitatory signal function ( $r(x)$ , in equations (62) & (63)) is defined by:

$$r(x) = \frac{x^4}{x^4 + 0.2^4}. \quad (64)$$

The inhibitory sigmoidal function ( $o(x)$ , in equations (62) & (63)) given by:

$$o(x) = \frac{x^2}{x^2 + 0.5^2}. \quad (65)$$

Using the same excitatory and inhibitory sigmoidal functions for SC-activated and FEF-activated cerebellar cells biases the network such that that FEF activity gets more preference if the maximal activities of FEF output cells and SC burst cells are out of sync. That is, the output

saccade vector will not be a vector average, but will be more biased towards the vector represented by the maximally active FEF output cell.

Cerebellar learning corrects movement errors via adaptive gain control. For example, if the saccadic target was at position  $(10^\circ, 10^\circ)$  and the saccade landed the eye at  $(9^\circ, 11^\circ)$  from its original position, then the retinotopic error is  $(1^\circ, -1^\circ)$ . The error  $B_\theta$ , where  $\theta = 0^\circ, 90^\circ, 180^\circ$ , or  $270^\circ$ , is calculated by breaking the retinotopic location into its constituent horizontal and vertical components. Thus the error takes the values:  $B_{0^\circ} = 1$ ,  $B_{90^\circ} = -1$ ,  $B_{180^\circ} = 0$  and  $B_{270^\circ} = 0$  when the eye foveates after moving  $9^\circ$  to right and  $11^\circ$  upwards. Learning is triggered in the cerebellum by the error-driven teaching signals  $\gamma_\theta$ , and is given by:

$$\gamma_\theta = B_\theta. \quad (66)$$

The teaching signal is on for just a single integration step. The adaptive weights learn when both the teaching and the sampling signals are present. Opponent learning ( $\gamma_\theta - \gamma_\Theta$ ) allows weights to either increase or decrease and thus correct saccadic undershoots or overshoots (Grossberg and Kuperstein, 1986). The learning rules for weights mediating the FEF-activated cells ( $W_{ij}^F$ ), SC-activated cerebellar cells ( $W_{ij}^S$ ) and DLPN cells ( $W_{ij}^D$ ) are given by:

$$\frac{dW_{ij}^S}{dt} = 67.5c_{ij}^S(\gamma_\theta - \gamma_\Theta), \quad (67)$$

$$\frac{dW_{ij}^F}{dt} = 67.5c_{ij}^F(\gamma_\theta - \gamma_\Theta), \quad (68)$$

$$\frac{dW_{vd}^D}{dt} = 67.5p_{vd}^D(\gamma_\theta - \gamma_\Theta), \quad (69)$$

*PPRF Cells:* Equations defining saccade generator cell activities are similar to equations present in Gancarz and Grossberg (1999). The saccadic drive ( $I_\theta^S$ ) is calculated by adding direct SC input with the cerebellar input and is described by:

$$I_\theta^S = 120\left(\sum_{j=1}^N \sum_{i=1}^N (c_{ij}^S W_{ij}^S + c_{ij}^F W_{ij}^F) + \sum_d \sum_v p_{vd}^D W_{vd}^D + 4K^B + 4K^U\right). \quad (70)$$

Saccadic input from the cerebellum is the sum of all weighed activities of FEF ( $c_{ij}^F$ ), SC ( $c_{ij}^S$ ) and DLPN ( $p_{vd}^D$ ) signals. The direct projections from the SC burst cells ( $K^B$ ) and SC buildup layers ( $K^U$ ) pass through sigmoidal transfer functions defined by equation (71) and (72), respectively:

$$K^B = \frac{b_{ij}^3}{0.4^3 + b_{ij}^3} \quad (71)$$

and

$$K^U = \frac{u_{ij}^3}{0.1^3 + u_{ij}^3}. \quad (72)$$

The turning points (0.4 and 0.1) of the sigmoidal functions ( $K^B$  and  $K^U$ ) were chosen so that, in case FEF is lesioned, there will be enough drive from SC to initiate a saccade.

*Long lead burst cells (LLBNs)*: LLBNs form the input stage for the saccade generator. They receive input from cerebellum and SC. They provide accelerate and brake signals needed for saccade initiation and termination. The LLBN activities ( $l_\theta$ ) obey the equation:

$$\frac{dl_\theta}{dt} = -1.3l_\theta + I_\theta^S - 2I_\Theta^S - 2b_\theta. \quad (73)$$

In (73),  $\Theta$  indicates the opposite direction and is defined as  $\Theta = \theta + 180$ .

The LLBN activity follows a push-pull opponent mechanism. It is excited by saccadic drive along its preferred direction ( $I_\theta^S$ ) and is inhibited by both the saccadic drive along the opponent direction ( $2I_\Theta^S$ ) and by the inhibitory burst neurons (term  $2b_\theta$ , see equation (75)). Stronger coefficients for the inhibitory inputs ( $2I_\Theta^S$  and  $2b_\theta$ , twice the excitatory input  $I_\theta^S$ ) are needed to achieve fast and accurate braking and thereby help in saccade termination.

*Excitatory burst neurons (EBNs)*: EBNs receive input from LLBNs and are inhibited by the OPNs. As long as EBNs are active, the eye keeps moving. EBN cell activities ( $e_\theta$ ) are modeled as:

$$\frac{de_\theta}{dt} = -3.5e_\theta + (2 - e_\theta)(5l_\theta + 1) - (1 + e_\theta)(2l_\Theta + 20v(o)). \quad (74)$$

Excitatory input comes from the agonistic LLBNs ( $l_\theta$ ) as well as an arousal signal (set equal to 1). Antagonistic LLBNs ( $l_\Theta$ ) and OPNs ( $v(o)$ , see equation (28)) inhibit the cell.

*Inhibitory burst neurons (IBNs)*: IBN cell activities ( $b_\theta$ ) form a negative feedback loop that controls the amplitude and duration of LLBN activity. They obey the equation:

$$\frac{db_\theta}{dt} = -15b_\theta + 50e_\theta. \quad (75)$$

The Inhibitory burst neurons are excited by the agonistic EBNs ( $e_\theta$ ) and send inhibitory feedback to the agonistic LLBNs ( $l_\theta$ , equation (73)).

*Tonic Neurons*: Tonic neurons integrate the EBN burst ( $e_\theta$ ) and pursuit ( $h_\theta$ ) cell outputs via push-pull opponent organization:

$$\frac{dt_\theta}{dt} = 0.3(e_\theta - e_\Theta) + 0.15(h_\theta - h_\Theta). \quad (76)$$

Eye position ( $\Psi$ ) is changed using the following formula:

$$\Psi = 20(t_\theta - t_\Theta). \quad (77)$$

Opponency ( $t_\theta - t_\Theta$ ) allows the eye to change its direction smoothly while tracking a target which makes sudden changes in its direction of motion.

**References:**

- Albright, T. D. (1984). Direction and orientation selectivity of neurons in visual area MT of the macaque. *J Neurophysiol*, 52(6), 1106-1130.
- Andersen, R. A., Asanuma, C., Essick, G., & Siegel, R. M. (1990). Corticocortical connections of anatomically and physiologically defined subdivisions within the inferior parietal lobule. *J Comp Neurol*, 296(1), 65-113.
- Arakawa, G. (2003). *An adaptive model of smooth pursuit eye movements*. Boston University, Boston.
- Barbas, H., & Mesulam, M. M. (1981). Organization of afferent input to subdivisions of area 8 in the rhesus monkey. *J Comp Neurol*, 200(3), 407-431.
- Basso, M. A., Krauzlis, R. J., & Wurtz, R. H. (2000). Activation and inactivation of rostral superior colliculus neurons during smooth-pursuit eye movements in monkeys. *J Neurophysiol*, 84(2), 892-908.
- Basso, M. A., & Wurtz, R. H. (2002). Neuronal Activity in Substantia Nigra Pars Reticulata during Target Selection. *J. Neurosci.*, 22(5), 1883-1894.
- Blatt, G. J., Andersen, R. A., & Stoner, G. R. (1990). Visual receptive field organization and cortico-cortical connections of the lateral intraparietal area (area LIP) in the macaque. *J Comp Neurol*, 299(4), 421-445.
- Blohm, G., Missal, M., & Lefevre, P. (2003). Interaction between smooth anticipation and saccades during ocular orientation in darkness. *J Neurophysiol*, 89(3), 1423-1433.
- Blohm, G., Missal, M., & Lefevre, P. (2005). Direct evidence for a position input to the smooth pursuit system. *J Neurophysiol*, 94(1), 712-721.
- Brodal, P. (1980a). The cortical projection to the nucleus reticularis tegmenti pontis in the rhesus monkey. *Exp Brain Res*, 38(1), 19-27.
- Brodal, P. (1980b). The projection from the nucleus reticularis tegmenti pontis to the cerebellum in the rhesus monkey. *Exp Brain Res*, 38(1), 29-36.
- Brown, J. W., Bullock, D., & Grossberg, S. (2004). How laminar frontal cortex and basal ganglia circuits interact to control planned and reactive saccades. *Neural Netw*, 17(4), 471-510.
- Buttner-Ennever, J. A., & Horn, A. K. (1997). Anatomical substrates of oculomotor control. *Curr Opin Neurobiol*, 7(6), 872-879.
- Carpenter, G. A., & Grossberg, S. (1993). Normal and amnesic learning, recognition and memory by a neural model of cortico-hippocampal interactions. *Trends Neurosci*, 16(4), 131-137.
- Chou, I. H., Sommer, M. A., & Schiller, P. H. (1999). Express averaging saccades in monkeys. *Vision Res*, 39(25), 4200-4216.
- Churchland, A. K., & Lisberger, S. G. (2005). Discharge properties of MST neurons that project to the frontal pursuit area in macaque monkeys. *J Neurophysiol*, 94(2), 1084-1090.
- Collins, C. E., Lyon, D. C., & Kaas, J. H. (2005). Distribution across cortical areas of neurons projecting to the superior colliculus in new world monkeys. *Anat Rec A Discov Mol Cell Evol Biol*, 285(1), 619-627.
- Davidson, R. M., & Bender, D. B. (1991). Selectivity for relative motion in the monkey superior colliculus. *J Neurophysiol*, 65(5), 1115-1133.
- de Brouwer, S., Missal, M., Barnes, G., & Lefevre, P. (2002). Quantitative analysis of catch-up saccades during sustained pursuit. *J Neurophysiol*, 87(4), 1772-1780.
- de Brouwer, S., Missal, M., & Lefevre, P. (2001). Role of retinal slip in the prediction of target motion during smooth and saccadic pursuit. *J Neurophysiol*, 86(2), 550-558.

- de Brouwer, S., Yuksel, D., Blohm, G., Missal, M., & Lefevre, P. (2002). What triggers catch-up saccades during visual tracking? *J Neurophysiol*, 87(3), 1646-1650.
- Dominey, P. F., & Arbib, M. A. (1992). A cortico-subcortical model for generation of spatially accurate sequential saccades. *Cereb Cortex*, 2(2), 153-175.
- Droulez, J., & Berthoz, A. (1991). A neural network model of sensoritopic maps with predictive short-term memory properties. *Proc Natl Acad Sci U S A*, 88(21), 9653-9657.
- Eggert, T., Guan, Y., Bayer, O., & Buttner, U. (2005). Saccades to moving targets. *Ann N Y Acad Sci*, 1039, 149-159.
- Everling, S., Pare, M., Dorris, M. C., & Munoz, D. P. (1998). Comparison of the discharge characteristics of brain stem omnipause neurons and superior colliculus fixation neurons in monkey: implications for control of fixation and saccade behavior. *J Neurophysiol*, 79(2), 511-528.
- Fries, W. (1984). Cortical projections to the superior colliculus in the macaque monkey: a retrograde study using horseradish peroxidase. *J Comp Neurol*, 230(1), 55-76.
- Gancarz, G., & Grossberg, S. (1999). A neural model of saccadic eye movement control explains task-specific adaptation. *Vision Res*, 39(18), 3123-3143.
- Gandhi, N. J., & Keller, E. L. (1997). Spatial distribution and discharge characteristics of superior colliculus neurons antidromically activated from the omnipause region in monkey. *J Neurophysiol*, 78(4), 2221-2225.
- Gellman, R. S., & Fletcher, W. A. (1992). Eye position signals in human saccadic processing. *Exp Brain Res*, 89(2), 425-434.
- Giolli, R. A., Gregory, K. M., Suzuki, D. A., Blanks, R. H., Lui, F., & Betelak, K. F. (2001). Cortical and subcortical afferents to the nucleus reticularis tegmenti pontis and basal pontine nuclei in the macaque monkey. *Vis Neurosci*, 18(5), 725-740.
- Glickstein, M., Cohen, J. L., Dixon, B., Gibson, A., Hollins, M., Labossiere, E., et al. (1980). Corticopontine visual projections in macaque monkeys. *J Comp Neurol*, 190(2), 209-229.
- Gottlieb, J. P., Bruce, C. J., & MacAvoy, M. G. (1993). Smooth eye movements elicited by microstimulation in the primate frontal eye field. *J Neurophysiol*, 69(3), 786-799.
- Grossberg, S. (1973). Contour enhancement, short-term memory, and constancies in reverberating neural networks. *Studies in Applied Mathematics*, 52, 213-257.
- Grossberg, S. (1980). Biological competition: Decision rules, pattern formation, and oscillations. *Proc Natl Acad Sci U S A*, 77(4), 2338-2342.
- Grossberg, S. (1982). *Studies of mind and brain*. Amsterdam: Kluwer/Reidel.
- Grossberg, S. (2000). The complementary brain: unifying brain dynamics and modularity. *Trends Cogn Sci*, 4(6), 233-246.
- Grossberg, S. (2003). How Does the Cerebral Cortex Work? Development, Learning, Attention, and 3-D Vision by Laminar Circuits of Visual Cortex (Vol. 2, pp. 47-76).
- Grossberg, S., & Kuperstein, M. (1986). *Neural dynamics of adaptive sensory-motor control : ballistic eye movements*. Amsterdam ; New York ;
- Grossberg, S., & Kuperstein, M. (1989). *Neural dynamics of adaptive sensory-motor control: Expanded edition*. Elmsford, NY: Pergamon Press.
- Grossberg, S., Mingolla, E., & Pack, C. (1999). A neural model of motion processing and visual navigation by cortical area MST. *Cereb Cortex*, 9(8), 878-895.
- Grossberg, S., Roberts, K., Aguilar, M., & Bullock, D. (1997). A neural model of multimodal adaptive saccadic eye movement control by superior colliculus. *J Neurosci*, 17(24), 9706-9725.

- Guan, Y., Eggert, T., Bayer, O., & Buttner, U. (2005). Saccades to stationary and moving targets differ in the monkey. *Exp Brain Res*, *161*(2), 220-232.
- Harting, J. K. (1977). Descending pathways from the superior colliculus: an autoradiographic analysis in the rhesus monkey (*Macaca mulatta*). *J Comp Neurol*, *173*(3), 583-612.
- Hodgkin, A. L. (1964). The Ionic Basis of Nervous Conduction. *Science*, *145*, 1148-1154.
- Huerta, M. F., Krubitzer, L. A., & Kaas, J. H. (1987). Frontal eye field as defined by intracortical microstimulation in squirrel monkeys, owl monkeys, and macaque monkeys. II. Cortical connections. *J Comp Neurol*, *265*(3), 332-361.
- Jurgens, R., Becker, W., & Kornhuber, H. H. (1981). Natural and drug-induced variations of velocity and duration of human saccadic eye movements: evidence for a control of the neural pulse generator by local feedback. *Biol Cybern*, *39*(2), 87-96.
- Keller, E. L., Gandhi, N. J., & Weir, P. T. (1996). Discharge of superior collicular neurons during saccades made to moving targets. *J Neurophysiol*, *76*(5), 3573-3577.
- Krauzlis, R. J., Basso, M. A., & Wurtz, R. H. (2000). Discharge properties of neurons in the rostral superior colliculus of the monkey during smooth-pursuit eye movements. *J Neurophysiol*, *84*(2), 876-891.
- Krauzlis, R. J., & Miles, F. A. (1996a). Initiation of saccades during fixation or pursuit: evidence in humans for a single mechanism. *J Neurophysiol*, *76*(6), 4175-4179.
- Krauzlis, R. J., & Miles, F. A. (1996b). Transitions between pursuit eye movements and fixation in the monkey: dependence on context. *J Neurophysiol*, *76*(3), 1622-1638.
- Langer, T. P., & Kaneko, C. R. (1990). Brainstem afferents to the oculomotor omnipause neurons in monkey. *J Comp Neurol*, *295*(3), 413-427.
- Lee, W. J., & Galiana, H. L. (2005). An internally switched model of ocular tracking with prediction. *IEEE Trans Neural Syst Rehabil Eng*, *13*(2), 186-193.
- Leichnetz, G. R. (1981). The prefrontal cortico-oculomotor trajectories in the monkey. *J Neurol Sci*, *49*(3), 387-396.
- Leichnetz, G. R., Smith, D. J., & Spencer, R. F. (1984). Cortical projections to the paramedian tegmental and basilar pons in the monkey. *J Comp Neurol*, *228*(3), 388-408.
- Leichnetz, G. R., Spencer, R. F., Hardy, S. G., & Astruc, J. (1981). The prefrontal corticotectal projection in the monkey; an anterograde and retrograde horseradish peroxidase study. *Neuroscience*, *6*(6), 1023-1041.
- Lisberger, S. G. (1998). Postsaccadic enhancement of initiation of smooth pursuit eye movements in monkeys. *J Neurophysiol*, *79*(4), 1918-1930.
- Lisberger, S. G., Pavelko, T. A., & Broussard, D. M. (1994). Responses during eye movements of brain stem neurons that receive monosynaptic inhibition from the flocculus and ventral paraflocculus in monkeys. *J Neurophysiol*, *72*(2), 909-927.
- Lynch, J. C., Graybiel, A. M., & Lobeck, L. J. (1985). The differential projection of two cytoarchitectonic subregions of the inferior parietal lobule of macaque upon the deep layers of the superior colliculus. *J Comp Neurol*, *235*(2), 241-254.
- Maioli, M. G., Domeniconi, R., Squatrito, S., & Riva Sanseverino, E. (1992). Projections from cortical visual areas of the superior temporal sulcus to the superior colliculus, in macaque monkeys. *Arch Ital Biol*, *130*(3), 157-166.
- Maunsell, J. H., & Van Essen, D. C. (1983). Functional properties of neurons in middle temporal visual area of the macaque monkey. I. Selectivity for stimulus direction, speed, and orientation. *J Neurophysiol*, *49*(5), 1127-1147.

- May, P. J., & Porter, J. D. (1992). The laminar distribution of macaque tectobulbar and tectospinal neurons. *Vis Neurosci*, 8(3), 257-276.
- McKenzie, A., & Lisberger, S. G. (1986). Properties of signals that determine the amplitude and direction of saccadic eye movements in monkeys. *J Neurophysiol*, 56(1), 196-207.
- Missal, M., Coimbra, A., Lefevre, P., & Olivier, E. (2002). Further evidence that a shared efferent collicular pathway drives separate circuits for smooth eye movements and saccades. *Exp Brain Res*, 147(3), 344-352.
- Missal, M., & Keller, E. L. (2002). Common inhibitory mechanism for saccades and smooth-pursuit eye movements. *J Neurophysiol*, 88(4), 1880-1892.
- Munoz, D. P., & Wurtz, R. H. (1993a). Fixation cells in monkey superior colliculus. I. Characteristics of cell discharge. *J Neurophysiol*, 70(2), 559-575.
- Munoz, D. P., & Wurtz, R. H. (1993b). Fixation cells in monkey superior colliculus. II. Reversible activation and deactivation. *J Neurophysiol*, 70(2), 576-589.
- Munoz, D. P., & Wurtz, R. H. (1995a). Saccade-related activity in monkey superior colliculus. I. Characteristics of burst and buildup cells. *J Neurophysiol*, 73(6), 2313-2333.
- Munoz, D. P., & Wurtz, R. H. (1995b). Saccade-related activity in monkey superior colliculus. II. Spread of activity during saccades. *J Neurophysiol*, 73(6), 2334-2348.
- Mustari, M. J., Fuchs, A. F., & Wallman, J. (1988). Response properties of dorsolateral pontine units during smooth pursuit in the rhesus macaque. *J Neurophysiol*, 60(2), 664-686.
- Nagao, S., Kitamura, T., Nakamura, N., Hiramatsu, T., & Yamada, J. (1997). Differences of the primate flocculus and ventral paraflocculus in the mossy and climbing fiber input organization. *J Comp Neurol*, 382(4), 480-498.
- Newsome, W. T., Wurtz, R. H., & Komatsu, H. (1988). Relation of cortical areas MT and MST to pursuit eye movements. II. Differentiation of retinal from extraretinal inputs. *J Neurophysiol*, 60(2), 604-620.
- Ono, S., Das, V. E., Economides, J. R., & Mustari, M. J. (2005). Modeling of smooth pursuit-related neuronal responses in the DLPN and NRTP of the rhesus macaque. *J Neurophysiol*, 93(1), 108-116.
- Ono, S., Das, V. E., & Mustari, M. J. (2004). Gaze-related response properties of DLPN and NRTP neurons in the rhesus macaque. *J Neurophysiol*, 91(6), 2484-2500.
- Optican, L. M., & Quaia, C. (2002). Distributed model of collicular and cerebellar function during saccades. *Ann N Y Acad Sci*, 956, 164-177.
- Pack, C., Grossberg, S., & Mingolla, E. (2001). A neural model of smooth pursuit control and motion perception by cortical area MST. *J Cogn Neurosci*, 13(1), 102-120.
- Pare, M., & Guitton, D. (1994). The fixation area of the cat superior colliculus: effects of electrical stimulation and direct connection with brainstem omnipause neurons. *Exp Brain Res*, 101(1), 109-122.
- Rashbass, C. (1961). The relationship between saccadic and smooth tracking eye movements. *J Physiol*, 159, 326-338.
- Robinson, D. A., Gordon, J. L., & Gordon, S. E. (1986). A model of the smooth pursuit eye movement system. *Biol Cybern*, 55(1), 43-57.
- Roy, J. E., & Cullen, K. E. (2003). Brain Stem Pursuit Pathways: Dissociating Visual, Vestibular, and Proprioceptive Inputs During Combined Eye-Head Gaze Tracking. *J Neurophysiol*, 90(1), 271-290.

- Scudder, C. A., Moschovakis, A. K., Karabelas, A. B., & Highstein, S. M. (1996a). Anatomy and physiology of saccadic long-lead burst neurons recorded in the alert squirrel monkey. I. Descending projections from the mesencephalon. *J Neurophysiol*, *76*(1), 332-352.
- Scudder, C. A., Moschovakis, A. K., Karabelas, A. B., & Highstein, S. M. (1996b). Anatomy and physiology of saccadic long-lead burst neurons recorded in the alert squirrel monkey. II. Pontine neurons. *J Neurophysiol*, *76*(1), 353-370.
- Seidemann, E., & Newsome, W. T. (1999). Effect of spatial attention on the responses of area MT neurons. *J Neurophysiol*, *81*(4), 1783-1794.
- Spatz, W. B., & Tigges, J. (1973). Studies on the visual area MT in primates. II. Projection fibers to subcortical structures. *Brain Res*, *61*, 374-378.
- Suzuki, D. A., & Keller, E. L. (1984). Visual signals in the dorsolateral pontine nucleus of the alert monkey: their relationship to smooth-pursuit eye movements. *Exp Brain Res*, *53*(2), 473-478.
- Suzuki, D. A., Yamada, T., Hoedema, R., & Yee, R. D. (1999). Smooth-pursuit eye-movement deficits with chemical lesions in macaque nucleus reticularis tegmenti pontis. *J Neurophysiol*, *82*(3), 1178-1186.
- Suzuki, D. A., Yamada, T., & Yee, R. D. (2003). Smooth-pursuit eye-movement-related neuronal activity in macaque nucleus reticularis tegmenti pontis. *J Neurophysiol*, *89*(4), 2146-2158.
- Takagi, M., Zee, D. S., & Tamargo, R. J. (1998). Effects of Lesions of the Oculomotor Vermis on Eye Movements in Primate: Saccades. *J Neurophysiol*, *80*(4), 1911-1931.
- Tanaka, K., Sugita, Y., Moriya, M., & Saito, H. (1993). Analysis of object motion in the ventral part of the medial superior temporal area of the macaque visual cortex. *J Neurophysiol*, *69*(1), 128-142.
- Tanaka, M., & Lisberger, S. G. (2002a). Enhancement of multiple components of pursuit eye movement by microstimulation in the arcuate frontal pursuit area in monkeys. *J Neurophysiol*, *87*(2), 802-818.
- Tanaka, M., & Lisberger, S. G. (2002b). Role of arcuate frontal cortex of monkeys in smooth pursuit eye movements. I. Basic response properties to retinal image motion and position. *J Neurophysiol*, *87*(6), 2684-2699.
- Tanaka, M., Yoshida, T., & Fukushima, K. (1998). Latency of saccades during smooth-pursuit eye movement in man. Directional asymmetries. *Exp Brain Res*, *121*(1), 92-98.
- Thielert, C. D., & Thier, P. (1993). Patterns of projections from the pontine nuclei and the nucleus reticularis tegmenti pontis to the posterior vermis in the rhesus monkey: a study using retrograde tracers. *J Comp Neurol*, *337*(1), 113-126.
- Thier, P., & Ilg, U. J. (2005). The neural basis of smooth-pursuit eye movements. *Curr Opin Neurobiol*, *15*(6), 645-652.
- Tian, & Lynch, J. C. (1997). Subcortical input to the smooth and saccadic eye movement subregions of the frontal eye field in Cebus monkey. *J Neurosci*, *17*(23), 9233-9247.
- Tian, J. R., & Lynch, J. C. (1996a). Corticocortical input to the smooth and saccadic eye movement subregions of the frontal eye field in Cebus monkeys. *J Neurophysiol*, *76*(4), 2754-2771.
- Tian, J. R., & Lynch, J. C. (1996b). Functionally defined smooth and saccadic eye movement subregions in the frontal eye field of Cebus monkeys. *J Neurophysiol*, *76*(4), 2740-2753.
- Torigoe, Y., Blanks, R. H. I., & Precht, W. (1986). Anatomical studies on the nucleus reticularis tegmenti pontis in the pigmented rat. II. Subcortical afferents demonstrated by the

- retrograde transport of horseradish peroxidase. *The Journal of Comparative Neurology*, 243(1), 88-105.
- Treue, S., & Maunsell, J. H. (1999). Effects of attention on the processing of motion in macaque middle temporal and medial superior temporal visual cortical areas. *J Neurosci*, 19(17), 7591-7602.
- Tusa, R. J., & Ungerleider, L. G. (1988). Fiber pathways of cortical areas mediating smooth pursuit eye movements in monkeys. *Ann Neurol*, 23(2), 174-183.
- Van Donkelaar, P., & Drew, A. S. (2002). The allocation of attention during smooth pursuit eye movements. *Prog Brain Res*, 140, 267-277.
- Van Gelder, P., Lebedev, S., & Tsui, W. H. (1995). Predictive human pursuit and "orbital goal" of microstimulated smooth eye movements. *J Neurophysiol*, 74(3), 1358-1361.
- Van Gelder, P., Lebedev, S., & Tsui, W. H. (1997). Peak velocities of visually and nonvisually guided saccades in smooth-pursuit and saccadic tasks. *Exp Brain Res*, 116(2), 201-215.
- Waitzman, D. M., Ma, T. P., Optican, L. M., & Wurtz, R. H. (1991). Superior colliculus neurons mediate the dynamic characteristics of saccades. *J Neurophysiol*, 66(5), 1716-1737.
- Yamada, J., & Noda, H. (1987). Afferent and efferent connections of the oculomotor cerebellar vermis in the macaque monkey. *J Comp Neurol*, 265(2), 224-241.
- Yamada, T., Suzuki, D. A., & Yee, R. D. (1996). Smooth pursuitlike eye movements evoked by microstimulation in macaque nucleus reticularis tegmenti pontis. *J Neurophysiol*, 76(5), 3313-3324.
- Zee, D. S., Yamazaki, A., Butler, P. H., & Gucer, G. (1981). Effects of ablation of flocculus and paraflocculus of eye movements in primate. *J Neurophysiol*, 46(4), 878-899.

SMOOTH PURSUIT SYSTEM		SACCADIC SYSTEM	
Symbol	Stands For	Symbol	Stands For
$v(i,j)$	Retinal velocity input at position (i,j)	$r_{ij}$	Retinal input at position (i,j)
$m_{ijvd}^-$	MT <sup>-</sup> cells	$a_{ij}$	LIP cells
$m_{ijvd}^+$	MT <sup>+</sup> cells	$b_{ij}$	SC burst layer cell
$s_d^V$	MST <sub>V</sub> cells	$u_{ij}$	SC buildup layer cell
$s_d^D$	MST <sub>D</sub> cells	$u_{ff}$	SC fixation cell
$f_d^I$	FPA input cells	$f_{ij}^I$	FEF Planning layer cells
$f_d^S$	FPA summation cells	$f_{ij}^O$	FEF output layer cells
$f_d^O$	FPA output cell	$f_{ff}^I$	FEF fixation layer cell
$g^P$	Signal reflecting target choice for SPEM by a cortico-BG-thalamo-cortical loop	$g^P$	Signal reflecting target choice for SAC by a cortico-BG-thalamo-cortical loop
$p_{vd}^D$	DLPN cells	$n_{ij}$	Nigral cell
$p_{ad}^N$	NRTP acceleration cells	$c_{ij}^F$	Cerebellar controlled FEF input
$p_{vd}^N$	NRTP velocity cells	$c_{ij}^S$	Cerebellar controlled SC input
$W_{vd}^D$	Adaptive weights between DLPN and saccadic part of Cerebellum	$W_{ij}^S, W_{ij}^F$	Adaptive weights for both horizontal and vertical saccades from cerebellum for SC and FEF signal
$I_\theta^P$	Pursuit drive along $\theta$	$I_\theta^S$	Saccade drive along $\theta$
$c_d^P$	Cerebellar pursuit cells	$l_\theta$	Long lead Burst cells along $\theta$
$h_\theta$	Pursuit neurons along $\theta$	$e_\theta$	Excitatory Burst cells along $\theta$

**Table 1.** Symbols of the commonly used cells and connection weights in the simulations.

<b>Symbol</b>	<b>Represents</b>
$\theta$	Directions along which the muscle can move the eye
$d$	Directions along which the target can move
$t_\theta$	Tonic neuron activity along $\theta$
$o$	Omnipauser neuron activity
$\Psi$	Eye Position

**Table 2:** Symbols that are common to both SAC and SPEM systems.

Connection in Model	Functional Interpretation	References
LIP to FEF , FEF to LIP	Saccadic target selection	(Barbas & Mesulam, 1981; Huerta et al., 1987)
FEF to SC, SC to FEF	Planned saccade information	(Fries, 1984; Huerta et al., 1987; Leichnetz, 1981; Leichnetz, Spencer, Hardy, & Astruc, 1981)
LIP to SC, SC to LIP	Saccadic target priming information	(Lynch, Graybiel, & Lobeck, 1985)
FEF to PPRF	Motor Command for saccade generation	(Huerta et al., 1987; Leichnetz, Smith, & Spencer, 1984)
SC to PPRF	Motor Command for saccade generation	(Harting, 1977; May & Porter, 1992; Scudder, Moschovakis, Karabelas, & Highstein, 1996a, 1996b)
SC to CBM	Saccadic Command for Fine Tuning	
SC to cNRTP		(Harting, 1977)
cNRTP to Vermis		(Thielert & Thier, 1993; J. Yamada & Noda, 1987)
MT to MST, MST to MT	Target Velocity signal is constructed	(Tusa & Ungerleider, 1988)
MST to DLPN	Target and background speed and direction input is projected	(Glickstein et al., 1980; Mustari et al., 1988; Ono et al., 2004; Suzuki & Keller, 1984)
MST to FPA	Direction and speed sensitive of target data	(Churchland & Lisberger, 2005; Maioli et al., 1992; Tian & Lynch, 1997; J. R. Tian & Lynch, 1996a, 1996b; Tusa & Ungerleider, 1988)
FPA to rNRTP	Direction sensitive target input reach eye acceleration cells in rNRTP.	(Suzuki et al., 1999; Suzuki et al., 2003; T. Yamada et al., 1996)
DLPN to CBM	Target and background speed and direction input is transferred.	(Mustari et al., 1988; Ono et al., 2005; Ono et al., 2004)
DLPN to Vermis		(Thielert & Thier, 1993; J. Yamada & Noda, 1987)
DLPN to VPF		(Nagao, Kitamura, Nakamura, Hiramatsu, & Yamada, 1997)
rNRTP to CBM (floccular complex)	Specific target data is transferred to CBM	(Giolli et al., 2001; Suzuki et al., 1999; T. Yamada et al., 1996)
CBM(floccular complex) to MVN/vLVN	Smooth pursuit Signal	(Lisberger, Pavelko, & Broussard, 1994; Roy & Cullen, 2003)
MVN/vLVN to NRTP	Eye velocity feedback signal	(Torigoe et al., 1986)
LIP to MT/MST	Saccadic target selection information is passed to SPEM system	(Andersen, Asanuma, Essick, & Siegel, 1990; Blatt, Andersen, & Stoner, 1990)
MT to SC	Foveo-fugal speed sensitive input to rostral fixation cells	(Fries, 1984; Maioli et al., 1992; Spatz & Tigges, 1973)

**Table 3.** Model neurons and their empirically determined connectivity and physiological properties.